

Development of a Combined Interface and Extended Finite Element Method to Predict Delamination in Composite Structures

by
Emmanuel Irizarry Zapata

A thesis submitted in partial fulfillment of the requirements for the degree of

Master in Science
in
Mechanical Engineering

UNIVERSITY OF PUERTO RICO
MAYAGÜEZ CAMPUS

December 2015

Approved by:

Vijay K. Goyal, Ph.D.
President, Graduate Committee

Date

Ricky Valentín, Ph.D.
Member, Graduate Committee

Date

Gustavo Gutiérrez, Ph.D.
Member, Graduate Committee

Date

Ricky Valentín, Ph.D.
Chairperson of the Department

Date

Paul Castillo, Ph.D.
Representative of the Office of Graduate Studies

Date

Copyright © December 2015
by
Emmanuel Irizarry Zapata and Vijay K. Goyal

The author has used his best effort in preparing this thesis. These efforts include the development, research, and testing of the theories and formulas to determine their effectiveness. The author shall not be liable in any event for incidental or consequential damages in connection with, or arising out of, the furnishing, performance, or use of these formulas.

Type Set in Times Roman 12 pt using L^AT_EX.

Development of a Combined Interface and Extended Finite Element Method to Predict Delamination in Composite Structures

Emmanuel Irizarry Zapata

Master in Science in Mechanical Engineering

University of Puerto Rico at Mayagüez

Dr. Vijay K. Goyal, Faculty Advisor, Mechanical Engineering

(ABSTRACT)

For this work, an user-defined element (UEL) in ABAQUS was developed in conjunction with a triangular traction separation law, as the Cohesive Zone Model, that combines the Extended Finite Element and Cohesive Element Methods to predict delamination in bonded cantilever beams. The UEL was written in FORTRAN to work within the ABAQUS environment. The major advantage of this approach is that the crack path, or delamination, is efficiently modeled by combining the best of the two methods. The model matches the experimental data with 1–7% of difference while matching the exact maximum displacement and capturing the nonlinear pattern behavior of the load-deflection curve.

Desarrollo de un Método Combinado de Elementos de Interface y Finitos para Predecir Delaminación en Estructuras Compuestas

Emmanuel Irizarry Zapata

Maestría en Ciencia en Ingeniería Mecánica

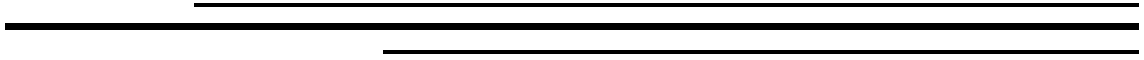
Universidad de Puerto Rico en Mayagüez

Dr. Vijay K. Goyal, Profesor Consejero, Ingeniería Mecánica

(RESUMEN)

En este trabajo, con la intención de modelar delaminación, desarrollamos un elemento definido por el usuario (UEL) usando el programa ABAQUS donde integramos un modelo de separación triabgular, como el model de zonas coesivas, que combina el Método de Elementos Finitos Extendidos y el Método de Elementos Coesivos. El UEL fue desarrollado en FORTRAN para poder trabajar con ABAQUS. La ventaja sobresaliente de este método es que la se puede modelar de forma efectiva el paso de propagación de la grieta, o delaminación. Esto se logra al poder combinar ambos métodos. Nuestro modelo puede predecir la data experimental, con una diferencia porcentual de 1–7% mientras puede capturar el comportamiento no lineal de la curva de desplazamiento y carga.

Dedication



To all my family

This page has been intentionally left blank.

Acknowledgments

First, I would like to express express my sincere gratitude to my advisor Dr. Goyal for his constant support during my research, for the opportunity, his patience and motivation. I will always be thankful for your confidence and trust in my skills and abilities.

I want to thank the Department of Mechanical Engineering and the Department of General Engineering of the University of Puerto Rico at Mayagüez (UPRM) for providing me with the Graduate Teaching Assistantship throughout my graduate studies. This research is affiliated with the Center for Aerospace and Unmanned Systems Engineering, a Center of Excellence of UPRM.

Also, I want to thank Dr. Ricky Valentín and Dr. Jorge Gustavo Gutiérrez for accepting to serve as my MS advisory committee. Finally, I would like to thank all my colleagues at the Mechanical Engineering Department for their support.

-Emmanuel

This page has been intentionally left blank.

Table of Contents

List of Figures	xi
List of Tables	xiii
List of Symbols and Abbreviations	xiv
Chapter 1. Preliminary Remarks	1
1.1 Motivation	1
1.1.1 Current State and Downfalls	1
1.1.2 The Need for a New Computational Technique	3
1.2 Project Description	3
1.2.1 Problem Description	3
1.2.2 Assumptions	5
1.2.3 Overall Goals	5
1.2.4 Intellectual Merit	6
1.2.5 Broader Impacts	7
1.3 Approach	8
1.3.1 Technical Approach	8
1.3.2 Development of Computational Technique	9
1.3.3 Thesis Outline	10
Chapter 2. Literature Review	11
2.1 Fracture Mechanics	11
2.1.1 Energy Considerations	15
2.1.2 Finite Element Approach	17
2.2 XFEM Approach	18
2.2.1 Background	18
2.2.2 Interfacial XFEM Implementations	20
2.3 Cohesive Zone Model	21

Chapter 3. ABAQUS UEL Implementation	23
3.1 FEM Element Formulation	24
3.2 XFEM Concepts	26
3.2.1 Level Sets: XFEM	26
3.2.2 XFEM Element Formulation	29
3.3 Cohesive Zone Model	35
3.3.1 Triangular Traction Separation Law	35
3.3.2 Exponential Traction Separation Law	37
3.4 Cohesive Element Method	38
3.4.1 Cohesive Element	38
3.4.2 Combined CE and XFEM	41
3.5 ABAQUS Capabilities	42
3.5.1 ABAQUS/Standard and ABAQUS/Explicit	42
3.5.2 Overview of ABAQUS Implementation	43
3.6 Implementing the Triangular Element	44
3.6.1 Writing a User Element (UEL)	44
3.6.2 Stiffness Matrix	46
3.6.3 ABAQUS Input File	47
3.7 Validation	48
3.7.1 Optimal Mesh and Tolerance	49
3.7.2 Experimental Setup	52
3.7.3 Benchmark 1: Analytical Solution	53
3.7.4 Benchmark 1: Numerical Simulation	55
3.7.5 Benchmark 2: Numerical Simulation Using Loading Blocks	58
3.7.6 Benchmark 3: Standard DCB using Normal Interfacial Strength by Song	61
Chapter 4. Final Remarks	63
4.1 Conclusion	63
4.2 Future Work	64
Appendix A. ABAQUS®GFROTRAN Environmental File	65
Appendix B. Input File Example	72
References	75
Vita	80

List of Figures

Figure 1.1	Finite Element crack tip refinement.	2
Figure 1.2	Double cantilever beam specimen.	4
Figure 1.3	Displacement δ calculation point.	4
Figure 1.4	Joints Configurations.	7
Figure 1.5	Proposed modules and their interactions	8
Figure 1.6	Workflow Development.	9
Figure 1.7	Proposed 1D XFEM Element (Element 3 and 4) interaction with 2D Elements	10
Figure 2.1	Infinite Plate with center crack $2a$	12
Figure 2.2	Fracture Modes I, II, III.	13
Figure 2.3	Near crack tip stress.	14
Figure 2.4	Adhesive and Cohesive Failure.	21
Figure 3.1	1D Set Spring Elements.	24
Figure 3.2	1D Set Spring Elements Plot using FEM.	25
Figure 3.3	Calculating SignDistance.	26
Figure 3.4	Signed Distance.	28
Figure 3.5	One-dimensional Set Spring Elements with a crack in the second element.	29
Figure 3.6	1D Set Spring Elements with Crack at second element using XFEM.	35
Figure 3.7	Triangular Traction Separation Law.	36
Figure 3.8	1D Set Spring Elements with Cohesive Crack using XFEM.	38
Figure 3.9	Cohesive Element Method.	40
Figure 3.10	Combined CE and XFEM.	41
Figure 3.11	ABAQUS/CAE Graphical User Interface.	43
Figure 3.12	ABAQUS/Standard Increment Flow.	45
Figure 3.13	Finite Element.	49
Figure 3.14	Augmented Finite Element Mesh.	49
Figure 3.15	Mesh Convergence.	50
Figure 3.16	Optimal Tolerance	51
Figure 3.17	Experimental Setup picture for DCB by Robinson (1992).	52
Figure 3.18	Double Cantilever Beam Specimen.	53

Figure 3.19	Load P vs. displacement δ - Delamination at Interface for DCB.	55
Figure 3.20	Benchmarks Comparison.	56
Figure 3.21	Error for Benchmark 1.	57
Figure 3.22	Double Cantilever Beam Specimen with loading blocks.	58
Figure 3.23	Load P vs. displacement δ - Delamination at Interface for DCB with load- ing blocks.	59
Figure 3.24	Error for Benchmark 2.	60
Figure 3.25	Load P vs. displacement δ - Delamination at Interface for DCB with load- ing blocks.	61
Figure 3.26	Error for Benchmark 3.	62

List of Tables

Table 3.1	Calculation of Φ and Ψ .	27
-----------	------------------------------------	----

List of Symbols and Abbreviations

ASTM	American Society for Testing and Materials
CEM	Cohesive Element Method
CEZ	Cohesive Element Zone
CZM	Cohesive Zone Model
DCB	Double Cantilever Beam
LSM	Level Set Method
UEL	Abbreviation for ABAQUS [®] user defined elements subroutine
XFEM	Extended Finite Element Method
n_{Γ}	Unit normal vector
G_{IC}	Mode I Energy Required to cause delamination
T_{ult}	Ultimate Traction Load

Chapter 1

Preliminary Remarks

Structural integrity is one of the most important aspects of a design process, especially when a component exhibit a flaw or a crack, in particular to structures with bonded interfaces. From a design point of view, crack detection and prediction is a critical factor that allows a designer to prevent a catastrophic failure. For this reason, engineers use modern techniques to improve the structural integrity and performance of structural components before the manufacturing them. The finite element methods have become a powerful method for these purposes. However the biggest challenges arise when discontinuities (i.e. voids, interfaces, cracks) are present within a structural component.

Two promising models can address this problem: cohesive element method (CEM) and the Extended Finite Element Method (XFEM). The Cohesive Zone Model (CZM) provides the traction-separation law needed for the crack opening. One advantage of CEM is that an there no need for an initial flaw. These elements do not reflect a visible crack. However, one limitation of CEM is that failure can only be simulated on the element boundaries. To solve this problem, the Extended Finite Element Method is used to overcome these difficulties to represent a crack in the element. XFEM has been used as a key tool to study fractures on structural components (Mubashar et al. 2014). The present work proposes to develop a hybrid finite element model using XFEM and CEM combined with Cohesive Zone Models to model delamination.

1.1 Motivation

1.1.1 Current State and Downfalls

There has been an interest in interfacial failure analysis. In fact, the aerospace community is focused on trying to understand the effects and behavior of cracks at potential locations. There has been much experimental work proofing the potential of the FEM for to calculate the crack opening threshold (Pommier et al. 2010; McClung and Newman 1999). Although FEM becomes the cornerstone in structural failure analysis, it fails to match the experimental data

even with complex mesh refinements and computational cost in large crack problems. The conventional methods require the user to conform the mesh to the cracked geometry because the crack tips cause a high-stress concentration, exhibiting large stresses and strains as a crack tip is approached.

For this reason, the problem will require a mesh refinement in the vicinity of the crack tip to obtain accurately stresses and strains as shown in Figure 1.1. For two-dimensional problems, it is recommended to use a circular contour around the crack tip typically filled with a quad-dominated mesh. This technique is available in commercial finite element software such as ABAQUS®, but is quite cumbersome and time-consuming due to the need of tediously complicated meshing techniques. The user must keep on track the amount of rings generated at the crack tip to report accurate quantities.

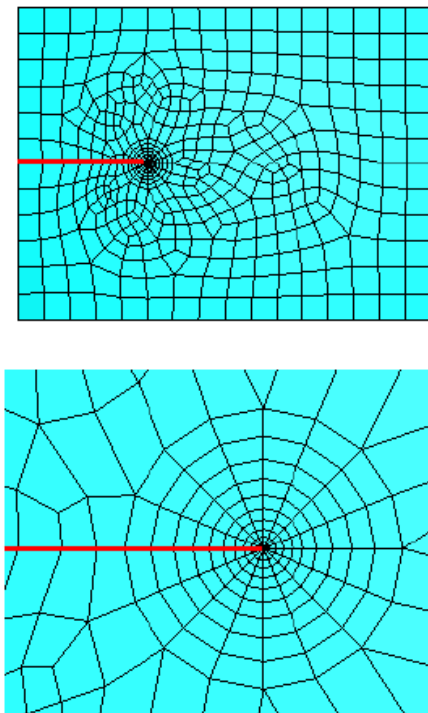


Figure 1.1: Finite Element crack tip refinement

1.1.2 The Need for a New Computational Technique

Stress and fracture mechanics based criteria present critical disadvantages (Martins da Silva and Öchsner 2008), especially for structures with interfacial bonds. Fracture mechanics relies on an initial crack size but in many applications, intuition can not predict the damage location point. Mesh dependency can be alleviated by using the proper enrichments to the FE model. Within the framework of the Extended Finite Element Method, using enrichment functions, it is possible to represent a crack in a structural component without the need of remeshing. However, XFEM has its technical challenges to predict interfacial failure. The enrichment functions are dependent on the type of analysis being executed because there is no general enrichment function applicable to all problems. On the other hand, Cohesive Elements present a very attractive. It is not necessary to predefine an initial crack unlike classical fracture mechanics approaches, and the damage takes place without the user intervention. Also, there has been a good agreement with experimental data for interfacial failure. CEM has been a successful technique used to predict delamination although discontinuities can only be modeled through the element boundaries.

The current implementation of cohesive elements in ABAQUS® has difficulties predicting the behavior of regions close to the interface. On the other hand, XFEM does not take into consideration material degradation. Moreover, highly localized stress concentrations and stress singularities exist in an adhesively bonded interfaces, even a mesh refinement does not provide a converged solutions (Mubashar et al. 2014). This is the main motivation for a need of new techniques. Thus, a combined XFEM-cohesive element model is needed to predict crack growth in the adhesive regions with mesh independence and at the same time predict changes in strength as the material start to degrade due to excessive loading, which is not possible using only cohesive elements. A combined model of XFEM and CEM will be attractive since it will be combining the advantages of both methods while reducing the drawbacks.

1.2 Project Description

1.2.1 Problem Description

Delamination is a major concern for bonded and composite structures. Discontinuities located at the interface zone of a structural component are difficult to predict. Classical computational techniques rely on cumbersome and time-consuming procedures.

A method that combines CEM and XFEM will be the key to address some of the numerical disadvantages. In order to provide a solution to this problem, the Double Cantilever Beam (DCB) as shown in Figure 1.2 is used to validate our implementation in ABAQUS with a custom UEL and input file.

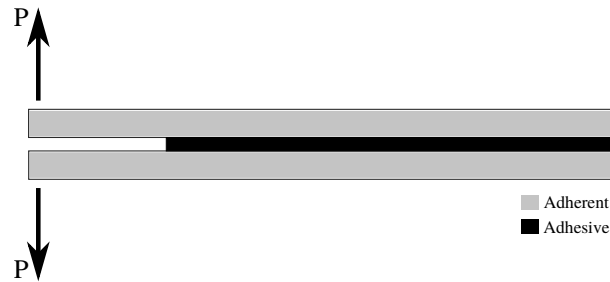


Figure 1.2: Double cantilever beam specimen

This type of joint consists of a composite material bonded by an epoxy adhesive. The DCB specimen is used to compute the values of G_{IC} for Mode I. The loading history consists of a predetermined displacement at the ends. The objective is to capture and numerically predict the load-displacement behavior at the crack opening point and demonstrate the robustness of the implementation. Figure 1.3 illustrates the location point at the opening for load P versus displacement δ data acquisition. When a constant load is applied, the value of δ increases accordingly.

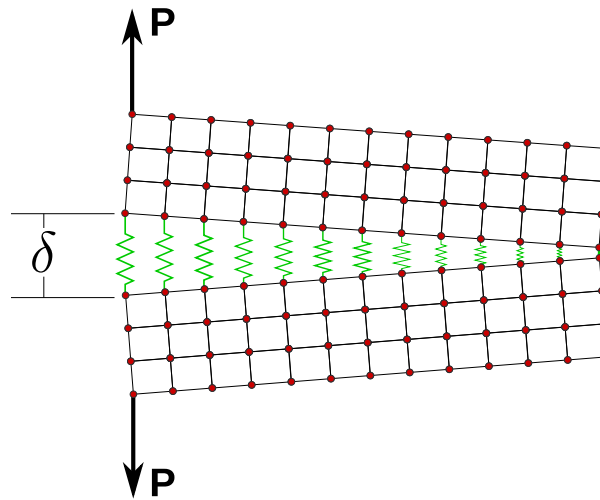


Figure 1.3: Displacement δ calculation point.

1.2.2 Assumptions

The following assumptions are made throughout the scope of this work:

1. Linear Elastic Fracture Mechanics (LEFM) approach is assumed.
2. Plane stress condition is assumed. Odi (2004) demonstrated that plane stress condition applies to relatively thin structures.
3. Substrate experience deformation due to tension. The influence of geometrical effects such as bond thickness is considered negligible. This condition limits our implementation to fracture Mode I.
4. Nonuniform shear stress at the overlap ends are ignored. This means that substrates are assumed to be effectively rigid. Fracture will only occur over a finite zone of the adhesive layer.
5. Adhesive stresses are assumed to be constant across the adhesive layer.
6. For the FEM simulation adhesive geometry is modeled as linear springs elements.

1.2.3 Overall Goals

The goal of this work is to develop a new interface element in combination with extended finite element method. The following tasks will be achieved in this work:

1. Study delamination for DCB specimens through computational techniques.
 - (a) Understand the effects of delamination
 - (b) Develop new theory using CEM and XFEM to model delamination.
2. Predict delamination on DCB specimens
 - (a) Construct a parametric input file using ABAQUS syntax.
 - (b) Implement the new element using a UEL, written in FORTRAN, for the ABAQUS environment.
3. Validate results using those available for the DCB in the literature.

The spring-like FE element capable of predicting failure at the material interfaces and crack growth propagation in Double Cantilever Beams using a combination of CEM and XFEM implemented through ABAQUS and a custom FORTRAN user subroutine (UEL). A customized FORTRAN environmental file written in PYTHON is provided in Appendix A.

1.2.4 Intellectual Merit

For application in aerospace environments, adhesively bonding composite structures involves more than just replacing the currently used methods like bolting and/or welding. Although not all structures are suitable for adhesive bonding, for some structures, consisting of dissimilar materials, adhesive bonding remains an excellent technique. A successful adhesive bond needs to be tailored to the structures loading conditions. In these sectors, the technology for design and engineering of durable composite adhesively bonded joints are further advanced, and its design relies mainly on experimental data. The main disadvantage of composite adhesive bonded joints is the limited knowledge available on the behavior of adhesively bonded joints applied to aircraft. Some experimental data is available for panels that debonded or cracked through the adhesive. The industries using these types of structural components will greatly benefit by using our state-of-the-art computational toolkit that will predict delamination of these composite-adhesive structures. This new element will efficiently improve information of the composite adhesive structural performance by integrating innovative finite element techniques, such as the CEM and XFEM, and promising constitutive laws for debonding.

A code that is efficient, reliable, and has a simple fracture algorithm has not been developed yet using ABAQUS. A code that combines XFEM and CEM will impact the scientific and/or engineering community, not to mention the major established industries such as aerospace, automobile, naval, chemical and petroleum companies. This work will enhance the understanding of bonded structures (adhesively bonded joints) such as the ones presented in Figure 1.4. In the context of adhesive joints, they offer advantages over traditional mechanical joint techniques (Pocius 2002).

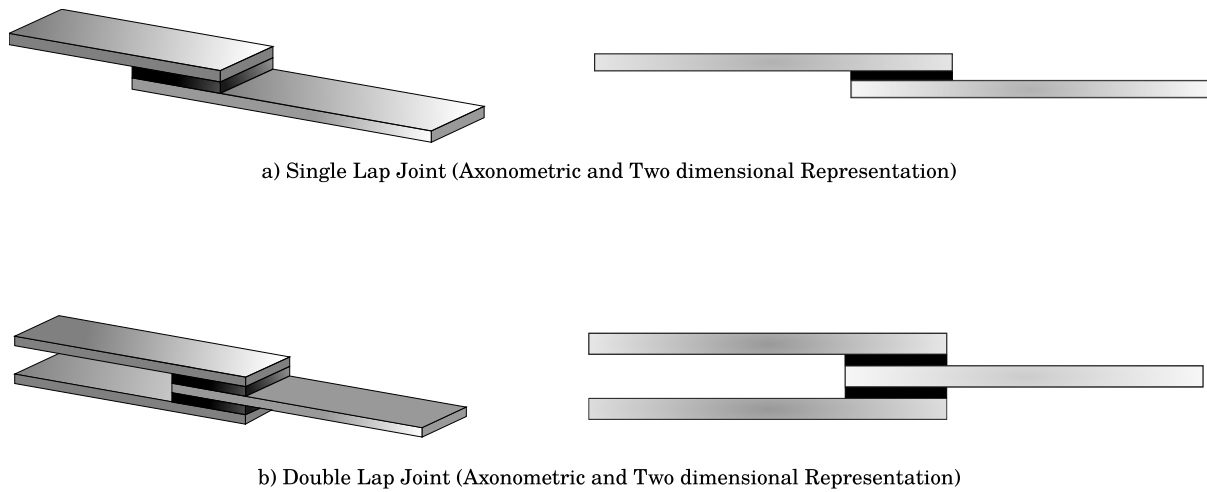


Figure 1.4: Joints Configurations

1.2.5 Broader Impacts

The implemented model will provide the basis to understand the weak physical interaction between metal-polymers and inorganic-polymer interfaces. The industry relies heavily on the usage of glues, our implementation can be used to simulate delamination.

1. **Automotive industry:** The application of adhesives and bonded joint in the automobile design improves the vehicle structure's performance. Some of the benefits are: (i) increases the stiffness of car body thus improving car's acoustics, (ii) overcomes durability problems by improving long-term durability, (iii) and enables downgauged steel and multi-material construction (Al, Mg, Composites) thus reducing the mass. Hence, this work will benefit the automotive industry. Also, our toolkit will fit their needs because it will interact with ABAQUS software used for the automotive applications.
2. **Ship structures:** Shipbuilding companies look for light-weight constructions and for constructions composed of various materials when welding technology reaches its limits. Some of the benefits are: (i) weight reduction, (ii) larger design space for light weight ships, (iii) electric and galvanic isolation, which prevents corrosion, (iv) and reduction of vibrations for high mechanical damping.
3. **Construction:** Modern light-weight design has revolutionized transportation construction over recent years. This has been possible due to the intelligent application of modern bonding technology. This has allowed the bonding of hitherto unrealizable combinations of materials in transportation construction, for example, the bonding of glass to steel,

aluminum with magnesium and the bonding of fiber-reinforced composite materials with metal. The knowledge obtained through this effort guarantees the reliability of adhesive bonds.

1.3 Approach

1.3.1 Technical Approach

The Figure 1.5 shows the proposed modules and their interactions

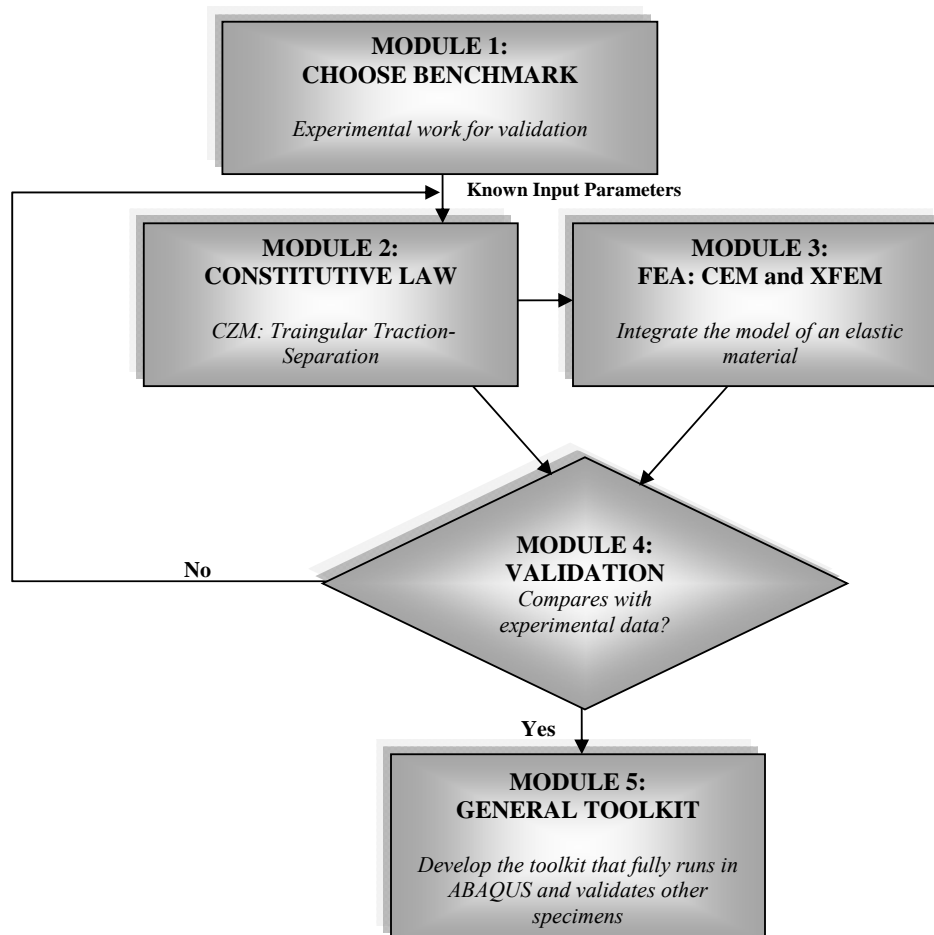


Figure 1.5: Proposed modules and their interactions

1.3.2 Development of Computational Technique

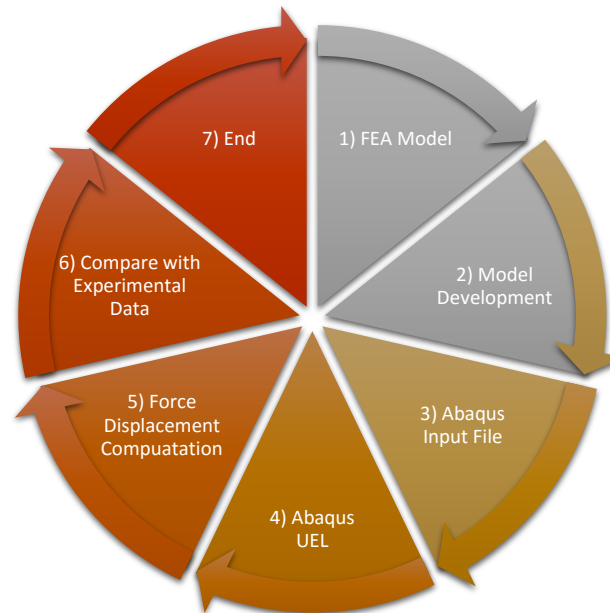


Figure 1.6: Workflow Development

The Figure 1.6 shows the general steps to accomplish our work. The first step is to define the boundaries of the model. The defined boundary conditions include the essential boundary conditions (displacements) and natural boundary conditions (tractions). The models are developed directly in ABAQUS input file in conjunction with the user-defined element (UEL) subroutine using FORTRAN. The UEL must interact with ABAQUS and the custom input file. After meshing, the domain consists of a set of enriched elements with additional shape functions that allow the separation and propagation in the event of the presence of a crack. However, ABAQUS has a limited element library that can be used with XFEM to simulate close to a real delamination. Thus, it is necessary to use Damage Models to control crack delamination during the simulation.

The predictive tool consisted of an algorithm programmed using ABAQUS with custom FORTRAN subroutines. In order to solve the problem, we proposed a combined CEM and XFEM model, as shown in Figure 1.7. The numbers in circles represent the element number, and the numbers without it represent the node location using a counterclockwise convention. Element number 3 and number 4 are the proposed element that connects 2-Dimensional quadrilateral elements. Vertical forces are applied at nodes 1 and 2 while node 7 and 8 remain fixed.

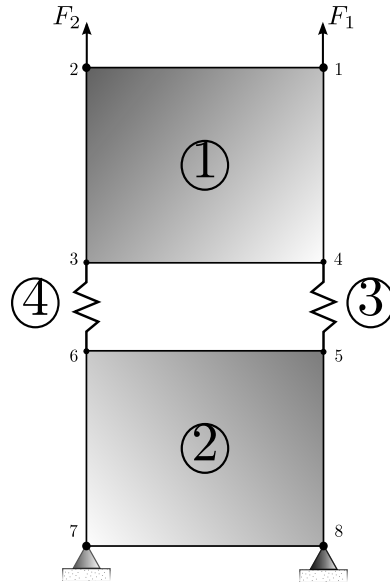


Figure 1.7: Proposed 1D XFEM Element (Element 3 and 4) interaction with 2D Elements

The idea is to implement an interface element with XFEM into ABAQUS using a UEL subroutine. The cohesive element is used for interfacial fracture while the XFEM is used for cracks propagating within the bulk interface. In order to validate the models, some published experimental work by Davies (2002), Robinson and Song (1992), and Song et al. (2008) are compared with the proposed model. Numerical results are presented for the analyzes of a Composite Double Cantilever Beam Specimen and for a problem involving multiple delamination for which comparisons are made with experimental results standardized by ASTM according to Robinson (1992).

1.3.3 Thesis Outline

This chapter is an introductory chapter explaining the problem we plan to solve with its motivations. Chapter 2 provides the literature review showing that this work is not found elsewhere. Chapter 3 provides the derivation of the element, its implementation, validation, and several case studies. Lastly, in Chapter 4 we provide the conclusions and various ideas to expand this work.

Chapter 2

Literature Review

Nowadays, many aerospace engineers are interested in a robust predictive technology for bonded joint structural interfaces. For over three decades, researchers have been trying to develop tools for *fracture analysis* of modern structures. Most traditional approaches require tens of thousands of degrees of freedom and tons of computing time, making the analysis impractical and/or very expensive (Kaiyuan et al. 2006) mainly due to the requirement of manual or adaptive mesh refinement. In the last decade, XFEM has become a very promising tool for this type of problems. The main advantage being that the mesh does not have to conform to the crack. The limitations of the XFEM can be compensated by combining the Cohesive Element Methods (CEM) that are also promising (Crocombe et al. 2008) to solve interfacial failure in adhesively bonded components.

2.1 Fracture Mechanics

The traditional approach for structural design is based on anticipating the applied stress and comparing the mechanical properties of the selected material. The material is considered for the application if its strength exceeds the applied stresses, a Factors of Safety is used to ensure this condition is met. However, fracture mechanics has three important aspects of the structural design: applied stress, flaw size, and fracture toughness. There are two key approaches to examine a fracture in the body: energy criteria and fracture toughness approach. Griffith (1921) was the first who proposed an energy criteria, modified by Irwin (1956).

Griffith (1921) defined the rate of change in potential energy located at the crack area as Energy Release Rate G . When the material exhibit a flaw (fracture) G becomes G_c , which represents the critical energy release rate, the responsible to measure fracture toughness. Figure 2.1 shows an infinite plate with a central crack of length $2a$ subjected to a remote tensile stress σ with thickness B . Griffith derived a parameter that describes the Energy Release Rate for this model as:

$$G = \frac{\pi a \sigma^2}{E} \quad (2.1)$$

where E is the Young's Modulus, σ the remotely applied stress, and a the half crack length. Now, when $G = G_c$ the critical stresses and crack size combine to produce a failure. The critical energy release rate for this case is described by:

$$G_c = \frac{\pi a_c \sigma_f^2}{E} \quad (2.2)$$

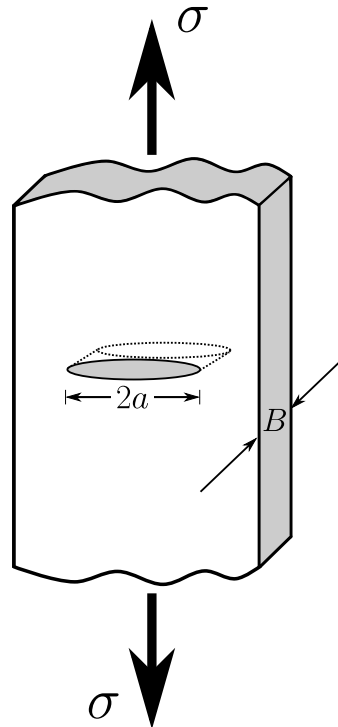


Figure 2.1: Infinite Plate with center crack $2a$.

Holding the values of G_c as constant and solving for σ_f the failure stress varies with $\frac{1}{\sqrt{a}}$. This criterion is based under the idea that a certain amount of energy G_c must be applied to create a critical flaw on the material, i.e., to create a new surface dA . The irreversible amount of energy during the creation of the surface are dA is written as:

$$dW = G_c dA \quad (2.3)$$

Equation 2.3 shows that in the case when the necessary amount of energy on a material is present, then it is sufficient to compensate the energy consumed in the creation of new surfaces (Pommier et al. 2010). If that energy is available, the direct consequence is crack propagation.

In other words, a crack is extended by a certain amount δa when the energy invested overcomes the material resistance to fracture.

The second traditional role of fracture mechanics is a systematic procedure that relies on calculating the fracture toughness and its growth rate with respect to the crack length. The classical overall objective is to determine the rate of change of the shape of an existing crack (Liu and Nairn 1999). The main objective of linear elastic fracture mechanics is to predict the critical loads that will cause a critical flaw to grow. The LEFM considers three fractures modes as shown on Figure 2.2: Mode I corresponds to normal opening and is the one emphasize in this work, Modes II and III are shear and sliding modes respectively. Mode I takes place when all the forces are perpendicular to the crack and pulling the lips of the specimen in opposite directions.

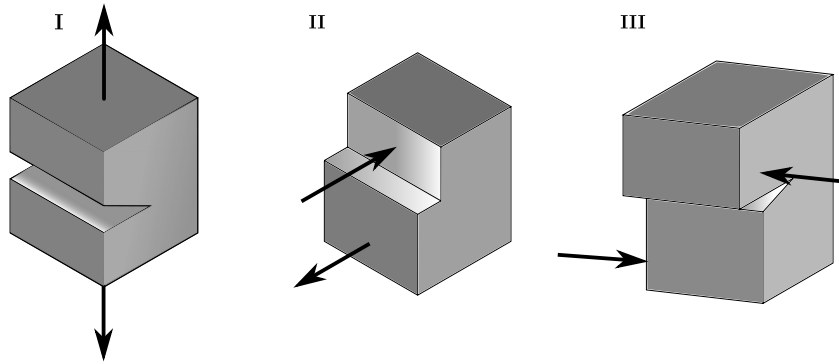


Figure 2.2: Fracture Modes I, II, III.

Figure 2.3 shows an element close to the crack tip in a linear elastic material, note that in-plane stresses are included. The calculation of the stresses, given by Equation 2.4, at this point A are proportional to a single constant value named K_I .

$$\begin{aligned}
 \sigma_{xx} &= \frac{K_I}{\sqrt{2\pi r}} \cos\left(\frac{\theta}{2}\right) \left[1 - \sin\left(\frac{\theta}{2}\right) \sin\left(\frac{3\theta}{2}\right) \right] \\
 \sigma_{yy} &= \frac{K_I}{\sqrt{2\pi r}} \cos\left(\frac{\theta}{2}\right) \left[1 + \sin\left(\frac{\theta}{2}\right) \sin\left(\frac{3\theta}{2}\right) \right] \\
 \tau_{xy} &= \frac{K_I}{\sqrt{2\pi r}} \cos\left(\frac{\theta}{2}\right) \sin\left(\frac{\theta}{2}\right) \cos\left(\frac{3\theta}{2}\right)
 \end{aligned} \tag{2.4}$$

When this value is known, the stress distribution can be obtained. This value is known as the fracture toughness K_I . If one assumes that at a certain amount of combined stresses the

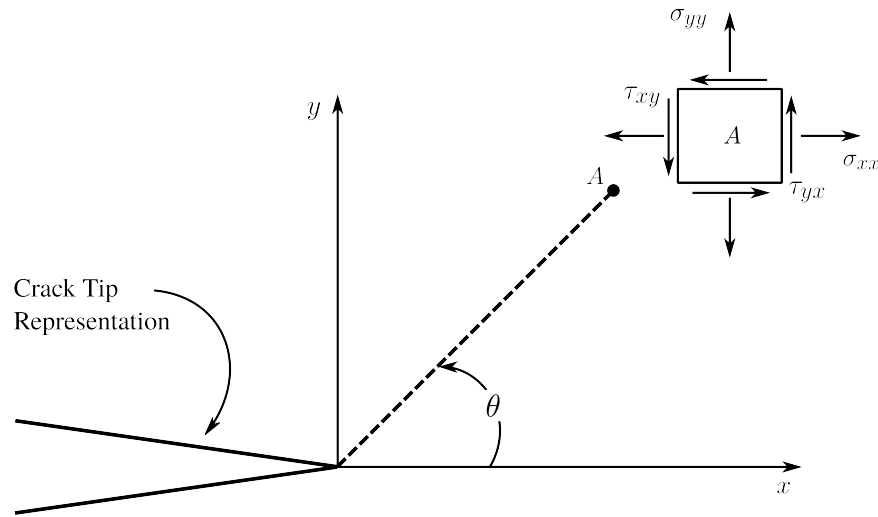


Figure 2.3: Near crack tip stress

material fails, and then it follows that fracture will occur at a critical fracture toughness K_{IC} .

For the infinite plate illustrated on Figure 2.1 the value of the fracture toughness is given by:

$$K_I = \sigma \sqrt{\pi a} . \quad (2.5)$$

In the vicinity of the crack at point A, the stresses in linear elasticity are singular according to

$$\sigma(r, \theta) = \sum_A K_A f_A^W(\theta) r^{\lambda_A} \quad (2.6)$$

The first terms of this expansion correspond to a linear combination of the three possible modes described by:

$$\sigma(r, \theta) = \sum_i K_i \frac{1}{\sqrt{2\pi r}} f_i(\theta) \quad (2.7)$$

The stresses tend to infinity when the value of the variable $r \rightarrow 0$. From a design perspective, fracture toughness argues that a material is capable of withstanding stresses up to a critical point described by the value K_{IC} . If the value of the fracture toughness is greater than K_{IC} the crack will propagate rapidly. In metallic materials, the crack propagation speed is close to the speed of sound. This critical value is an alternative measure of material fracture toughness. When flaws are present, the fundamental questions are: will the crack propagate under the given loading and environmental conditions; and, if it does propagate, it is possible to predict at what rate it propagates and what is the final configuration? Must the part be replaced? In general, these questions are answered through experiments. However, computational simulations are an

attractive, cost-effective method that is widely accepted as a key tool (Pommier et al. 2010).

2.1.1 Energy Considerations

Griffith (1921) derived a thermodynamic criterion for fracture by considering the total change in energy of a cracked domain in terms of the increase in crack length. His model satisfied certain critical energy criteria rather than a stress-based approach. For a crack domain subjected to arbitrary loading the first law of thermodynamics states that the change in total energy is proportional to the amount of performed work and the change of heat content:

$$\frac{d}{dt}(U_k + U_s + U_\Gamma) = \frac{d}{dt}(Q + W)$$

where U_k is the kinetic energy, U_s the total strain energy, U_Γ the surface energy, W the external work, and Q consists of the heat added to the system. For the case of adiabatic quasi-static system, Q and U_k are equal to zero:

$$\frac{d}{dt}(U_s + U_\Gamma) = \frac{d}{dt}(W) \quad (2.8)$$

The Eq. (2.8) can be re-written in terms of the crack half length a , as follows:

$$\frac{\partial W}{\partial a} = \frac{\partial U_s}{\partial a} + \frac{\partial U_\Gamma}{\partial a} \quad (2.9)$$

Equation 2.9 represents the energy balance during crack growth. It states that the work rate supplied to the continuum by the applied external load is equal to the surface energy dissipated during crack propagation, U_Γ , plus the rate of strain energy, U_s , decomposed into elastic U_s^e and plastic U_s^p parts

$$U_s = U_s^e + U_s^p \quad (2.10)$$

Using Variational and Energy Principles Equation 2.9 can be expressed in terms of the Total Potential Energy, Π :

$$\Pi = U_s^e - W \quad (2.11)$$

$$\begin{aligned} -\frac{\partial \Pi}{\partial a} &= -\frac{\partial U_s^e}{\partial a} + \frac{\partial W}{\partial a} \\ &= -\frac{\partial U_s^e}{\partial a} + \frac{\partial U_s}{\partial a} + \frac{\partial U_\Gamma}{\partial a} \\ &= \frac{\partial U_s^p}{\partial a} + \frac{\partial U_\Gamma}{\partial a} \end{aligned} \quad (2.12)$$

Therefore, the amount of energy that is available for the crack growth is compared with the resistance of the material that must be overcome for crack growth. On the other hand, it also indicates that the rate of decrease of potential energy during crack growth is equal to the rate of energy dissipated in plastic deformation and crack growth. However another practical way to express the crack domain is based on the Maximum Energy Release Rate. Adopting Irwin's generalized expression for the energy release rate,

$$G(\theta) = \frac{1}{E'} \left[K_I^2(\theta) + K_{II}^2(\theta) \right] \quad (2.13)$$

The evaluation of $G(\theta)$ for kinked crack becomes:

$$G(\theta) = \frac{1}{4E'} g^2(\theta) \left[\left(1 + 3 \cos^2 \theta\right) K_I^2 \right] + 8 \sin \theta \cos \theta K_I K_{II} + \left(9 - 5 \cos^2 \theta\right) K_{II}^2 \quad (2.14)$$

Moreover, the angle of crack propagation is found by minimizing $G(\theta)$:

$$\frac{\partial^2 G(\theta)}{\partial \theta^2} = 0 \quad (2.15)$$

Now, satisfying the instability condition,

$$\frac{\partial^2 G(\theta)}{\partial \theta^2} < 0 \quad (2.16)$$

Summarizing, the general form of the Equation 2.14 takes the following form,

$$G(\theta) = \frac{1}{E'} \left[A_{11} K_I^2(\theta) + 2A_{12} K_I(\theta) K_{II}(\theta) + A_{22} K_{II}^2(\theta) \right] \quad (2.17)$$

where

$$\begin{bmatrix} A_{11} \\ A_{12} \\ A_{22} \end{bmatrix} = g^2(\theta) \begin{bmatrix} 4 - 3 \sin^2 \theta \\ -2 \sin 2\theta \\ 4 + 5 \sin^2 \theta \end{bmatrix} \quad (2.18)$$

Taking into consideration that the proposed analysis will be restricted to structures with linear thermoelastic phases and uniform temperature gradients, the full thermal elasticity problem

can be treated as a superposition of two problems suggested by Liu (2007):

$$G = G_0 + \frac{V\Delta T}{2} \left(2 \frac{d(\sigma^m \alpha)}{dA} + \frac{d(\sigma^r \alpha)}{dA} \right) + \frac{d}{dA} \left(\int_{S_c} \underline{T}^r \underline{u}^m dS + \frac{1}{2} \int_{S_c} \underline{T}^r \underline{u}^r dS \right) \quad (2.19)$$

$$G_0 = \frac{d}{dA} \left(\frac{1}{2} \int_{S_c} \underline{T}^0 \underline{u}^m dS + \frac{1}{2} \int_{S_c} \underline{T}^m \underline{u}^0 dS + \frac{1}{2} \int_{S_c} \underline{T}^m \underline{u}^m dS \right) \quad (2.20)$$

where \underline{T} represent the surface tractions and displacements m and r refer to mechanical or residual stress terms, respectively, and α is the position-sensitive thermal expansion coefficient of the composite. The first term is the traditional energy release rate while the subsequent terms are required in many composite fracture problems to account for effects of residual stresses, traction-loaded cracks, and imperfect interfaces. Liu (2007)'s work describes a new energy analysis that extends and corrects the results in a previous adhesion study according to Equation 2.21.

$$G_0 = \frac{d}{dA} \left(\frac{1}{2} \int_{S_T} \underline{T}^0 \cdot \underline{u}^m dS - \frac{1}{2} \int_{S_u} \underline{T}^m \cdot \underline{u}^0 dS + \frac{1}{2} \int_{S_c} \underline{T}^m \cdot \underline{u}^m dS \right) \quad (2.21)$$

2.1.2 Finite Element Approach

The whole idea behind the FEA is to approximate the solution to a governing differential equation. There is an enormous range of software focused on solving a broad variety of problems such as structural mechanics, heat and mass transfer and fluid mechanics, just to name a few. The FEM effectiveness depends on the material properties of the structure under study. If the material behavior is linear and some geometrical restrictions are met, the field solution becomes straightforward with analytical or traditional computational techniques (Bialstrokecki et al. 2002). However, when the material and geometric behavior is nonlinear, the solution is limited, and traditional approaches become even more computationally expensive (Armentani and Citarella 2006).

There are currently two main approaches: (i) mesh-free methods (Rabczuk and Belytschko 2007), and (ii) those that require discretization but modify the mesh to adapt to the geometry evolution (Kettill et al. 2007). Adaptive FEM approaches permit completely arbitrary geometry of both structure and cracks by updating the mesh to conform to the evolving crack geometry. Simulation of crack growth is more complicated than many other applications of computational mechanics because the geometry of the structure evolves during the simulation (Maligno et al. 2010). For this reason, a geometric description of the body that is independent of any numerical discretization and can be maintained and updated as part of the simulation process

is preferred. In a non-geometrical approach, the material stiffness is appropriately degraded locally to mimic the displacement discontinuity created by a crack, while the underlying geometry and the mesh models are kept unchanged (Malvar and Fourney 1990).

In the classical FEM, it is necessary to refine the mesh near the crack tip and thus remeshing is a must even after crack propagation. However, some of the newer techniques, such as the XFEM, do not require remeshing to predict crack propagation. In the XFEM, the finite element formulation is enriched by the crack tip asymptotic displacements and by a Heaviside function to account for discontinuity in the displacement. Advances in the extended finite element method (XFEM) (Dolbow et al. 1999) are described in a general sense, as a method of introducing discontinuities and enrichments within the finite elements. This makes possible to model problems such as crack growth, dislocations, and shear bands.

In general, a crack can be modeled as a sharp crack or blunted crack. ABAQUS® offer several ways to model cracks. The most classical technique is based on conventional FEM. It requires constructing a mesh that includes the crack itself. The second is based on the XFEM approach. The XFEM method does not require the mesh to match exactly the crack geometry. For the sharp crack, the model is performed using a seam geometry (line on a 2D geometry). For blunted cracks, a finite strain analysis is considered. This approach is characterized by a non-singular behavior at the crack tip. A crack tip causes stress concentrations, for that reason, the stress gradients are large as a crack tip is approached. As a consequence, the finite element mesh must be refined at the vicinity of the crack tip to capture and monitor accurate stresses. This requirement increases the degrees of freedoms on the model and at the same time it increases the computation time.

2.2 XFEM Approach

XFEM has been improved during the past two decades to deal with strong and weak discontinuities. The main goal of crack propagation is to determine how will the structure fail. During the 1980's the evolution of components and meshing programs allowed a rapid development of crack propagation models.

2.2.1 Background

The XFEM approximation is an extension of a method that was developed during the 1970's. Due to the mathematical singularity present at the crack tip, it was necessary to develop a

methodology that takes into account the existing limitations. Benzley (1974) introduced the novel idea of “enrichment elements” applied to near tip field using FEM for static analysis. He formulated the first two-dimensional “enriched element” and derived a closed form asymptotic field formulation for crack tip displacements. However, in 1999 for the first time, a practical enriched finite element for crack propagation was applied and was called XFEM (Mohammadi 2012). Using XFEM, the standard displacement-based functions of FEM approximation are enriched by additional special functions that are based on the framework of Partition of Unity.

Some advantages of XFEM is that we do not need to conform the finite element mesh to the internal boundaries. Hence, a single mesh is sufficient to capture the material interfaces and cracks evolution. The main advantages are that the finite element framework is retained while using a single-field variational principle. The extended finite element method (XFEM) was developed by Belytschko and Black (1999) and the method was based on Babuska and Melenk (1996) to help alleviate the shortcomings of the finite element method. It has been used to model the propagation of various discontinuities: strong (cracks) and weak (material interfaces).

The motivation behind XFEM was to keep advantages of mesh-free methods while alleviating their negative aspects. One of the first applications was to model a fracture using discontinuous functions added to standard shape functions. The primary advantage was the no need to remesh and to be able to keep track of the crack path.

Simulating crack propagation using traditional finite element methods is challenging because the topology of the domain changes continuously. According to Vigneron et al. (2009), FEM has evolved to new applications, reducing computational costs due to remeshing procedures in FEM remains a major concern (Logé et al. 2007). In classical FEM, remeshing is done at each propagation step, making the numerical simulations computationally costly.

Möes (1999) used XFEM to create a technique for simulating crack propagation without remeshing the domain. In XFEM, if an adequate initial mesh about the crack size is constructed, remeshing is not needed for each propagation step. XFEM has also been combined with other techniques to increase performance and accuracy (Chahine et al. 2011) and has been used in combination with Level Set methods to track the moving discontinuity sets (Bordas and Moran 2006). However, the XFEM approach carries its technical challenges (Richardson et al. 2009). It is important to highlight that current XFEM involves using modern remeshing techniques to enhance further the solution without affecting the computational cost.

In general, two approaches for structural design and material selection are available. The first one is based on the approach of material strength. By comparing the anticipated design

stress-strain with the capabilities of the candidate material, an evaluation is performed if its strength prevents failure. The second one has three important variables: the applied stress, flaw size, and fracture toughness. The combinations of the above variables are quantified by the field of Fracture Mechanics. XFEM is based on the theory of Fracture Mechanics which analyzes if flaws or defects will grow into large enough cracks to cause the component to fail catastrophically. Many researchers have used mixed-mode fracture mechanics (Combescure et al. 2008; Grál'goire et al. 2007; Menk and Bordas 2010). However, the main drawback is the element re-meshing.

2.2.2 Interfacial XFEM Implementations

Xiao and Karihaloo (2014) developed a hybrid crack element (HCE) for the calculation of the fracture toughness and high-order coefficients of the Williams Expansion. The element was designed for each crack tip taking into consideration the whole domain and the HCE model general FE mesh and implemented into a commercial FE package LUSAS. Xiao and Karihaloo (2014) validated the model using several 2D classical cases. Richardson et al. (2009) presented a method that simulated a 2D crack propagation that combined the features of XFEM with an algorithm that cut triangulated domains. His work shows several advantages such as material connectivity that are essential for XFEM enrichment functions Ahmed (2009) presented a coupled XFEM and Level Set methodology to represent in full detail geometrical discontinuities. With this method, he was able to simulate moving interfaces and proposed to use it as a potential methodology for performing failure analysis. Chessa et al. (2002) presented an enriched element method for multidimensional Stefan problems. The enrichment presented was developed with a discontinuity in the derivative of the temperature normal to the interface. The method allowed to approximate a phase transformation within an element without the need of re-mesh accurately. Also, several examples were presented to demonstrate the robustness of the implementation. Chen et al. (1995) presented a smoothing procedure for XFEM with the objective to outperform the standard XFEM. His contribution eliminates the need for the mesh alignment with the crack and the re-meshing technique using Heaviside and asymptotic crack tip functions. He called the method Edge-based Smoothing, and it relies on generalized smoothing operation over smoothing domains.

2.3 Cohesive Zone Model

The current methods adopt a continuum approach to focus on the pre-failure process. With advances in numerical techniques, as well with computational capacity, we can use material models to simulate failure progression, Cohesive Zone Model being one of such models (Lu 2012). It is quite challenging to model mesoscale fracture that would take into account micro-crack initiation to mesocrack propagation. The CZM can do so by modeling transition from continua to discontinua of the material (Park 2007). During the crack growth process, two new surfaces are created. Before the crack is formed, these two surfaces are held together by traction within a cohesive zone. The traction varies relative to the displacement of the surfaces. A cohesive law describes the phenomena in the cohesive zone in terms of the traction and the separation of the surfaces during the fracture process. A cohesive law is also denoted a traction-separation law. The concept to describe the cohesive phenomena before fracture has been established for almost half a century ago. This model considers the relation between the traction and separation that are normal to the fracture surfaces, and the unphysical stress singularity at the crack tip in the traditional linear elastic fracture mechanics is removed. The cohesive models were later extended to the mode II fracture process, in which the tangential traction and separation are considered instead. Figure 2.4 illustrates the difference between adhesive failure and cohesive failure. In general, CZM takes care of the material's post-failure behavior.

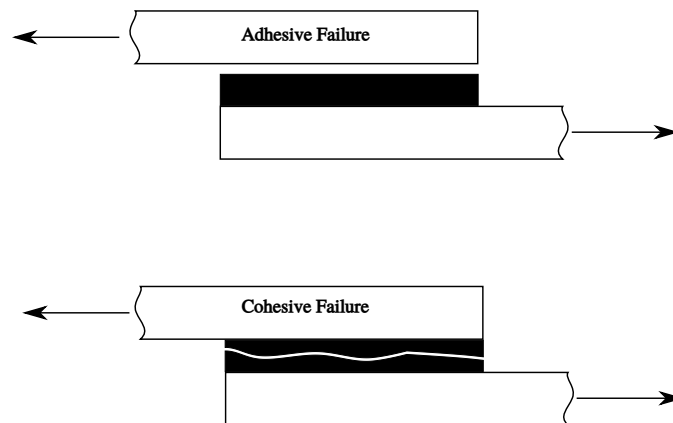


Figure 2.4: Adhesive and Cohesive Failure

CZM captures failure using computational methods such as Cohesive Element Method (CEM), Discrete Element Method (DEM), Extended Finite Element Method (XFEM), just to mention a few (Konuk 2009, 2010). In this work, we emphasize the cohesive law with XFEM

and CEM to characterize the failure on the adhesive.

We are challenged by current failure prediction techniques to model intra and interlaminar failure of laminated composites (Charles 2001). In general, the CZM is implemented at the beginning of the analysis where a traction-separation law (TSL) is set in place (Geubelle 1998; Camanho (2004); Xu 1994). These methods highly depend on the mesh, altering the structural stiffness. Some researchers have tried to address this issue without much success (Geubelle 1998; Song 2006; Blal 2011; Zavattieri 2001). The problem of mesh dependency has been studied by combining CZM and XFEM (Moës 2002; Dolbow 2001; Melenk 1996)

The drawback of using merely XFEM is that if the crack takes place at the node, the enrichment functions fail. CEM on the other hand only works at the nodes. Hence, a combined approach would allow us to capture the failure at any possible location without the need to remesh when combined with a CZM.

Chapter 3

ABAQUS UEL Implementation

In this work, we combine the Cohesive Element Method (CEM) and the eXtended Finite Element Method (XFEM) with Cohesive Zone Model (CZM) to solve the delamination in composite structures, as explained in Section 1.2. For the XFEM implementation, we use the enrichment with Heaviside functions and for the CZM, we use the triangular separation law. For efficient analysis using XFEM, we need an algorithm to detect the enriched nodes or elements. For the Heaviside enrichments, only the nodes that belong to an element split by a discontinuity may be used. Alternatively, a boundary zone close to the interface can well work for particular problems. However, the Heaviside enrichment approach is more convenient for the problems we are solving in this work.

In a typical finite element method, the geometry of the model is updated if a crack is initiated or an existing crack propagates. In contrast, XFEM required no remeshing when the crack propagates. In an updated Lagrangian formulation of large deformation analysis, however, the converged configuration of the model has to be updated by computed nodal displacements. The same is true the XFEM analysis. Thus, although there is no need for remeshing during a strong discontinuity, the geometry needs to be updated. In this context, XFEM needs a method to update and handle changes associated with evolving cracks, and changing their degrees of freedom while incorporating the CZM at the same time into the UEL.

We will begin by discussing an overview of the steps used to implement the a Triangular Model into ABAQUS® using an user-defined-element (UEL). The UEL implementation will be discussed in the derivation and development section. The Triangular Model will be validated using experimental data from the literature.

3.1 FEM Element Formulation

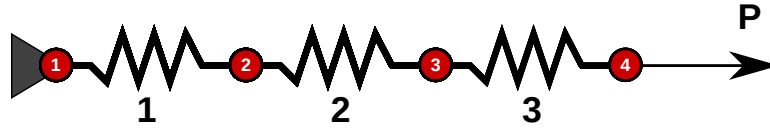


Figure 3.1: 1D Set Spring Elements

In order to provide a better understanding, let us start with a brief overview for the FEM. Consider the set of spring elements shown in Figure 3.1. Each spring element has a length of $L/3$ with an elastic modulus E and cross sectional area A . All other variables are stored in a single variable called κ . The node one is fixed while the prescribed load P is located at node four. The numbers in white represent the node numbers, the black numbers represent the element numbers. The goal is to find the displacements for all nodes

$$\delta = \begin{Bmatrix} u_1 \\ u_2 \\ u_3 \\ u_4 \end{Bmatrix} \quad (3.1)$$

The global stiffness of the system using standard FE approach is

$$K_G = \kappa \begin{bmatrix} 1 & -1 & 0 & 0 \\ -1 & 2 & -1 & 0 \\ 0 & -1 & 2 & -1 \\ 0 & 0 & -1 & 1 \end{bmatrix} \quad (3.2)$$

After the global stiffness for the springs sets is assembled, the linear system of equations can be written as

$$K_G \delta = P \quad (3.3)$$

where the P represents the external forces applied to the system, δ the unknown displacements at each node. For our example the Equation 3.3 becomes

$$\kappa \begin{bmatrix} 1 & -1 & 0 & 0 \\ -1 & 2 & -1 & 0 \\ 0 & -1 & 2 & -1 \\ 0 & 0 & -1 & 1 \end{bmatrix} \begin{Bmatrix} u_1 \\ u_2 \\ u_3 \\ u_4 \end{Bmatrix} = \begin{Bmatrix} P_1 \\ P_2 \\ P_3 \\ P_4 \end{Bmatrix} \quad (3.4)$$

After applying the essential and natural boundary conditions the Equation 3.4 and using using

Gauss elimination solving the equations we find the solution as follows:

$$\delta = \begin{Bmatrix} u_1 \\ u_2 \\ u_3 \\ u_4 \end{Bmatrix} = \begin{Bmatrix} 0 \\ P/3 \\ 2P/3 \\ P \end{Bmatrix} \quad (3.5)$$

Now, let $P = 30$ the displacement vector δ becomes:

$$\delta = \begin{Bmatrix} u_1 = 0 \\ u_2 = 10 \\ u_3 = 20 \\ u_4 = 30 \end{Bmatrix} \text{ Units} \quad (3.6)$$

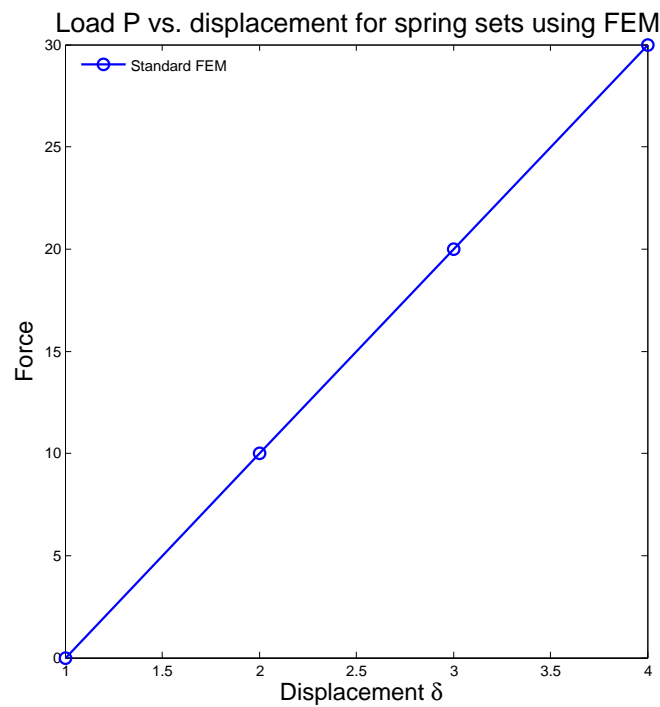


Figure 3.2: 1D Set Spring Elements Plot using FEM

Figure 3.2 shows, as expected, K is a linear relationship between the load P and the displacement δ according to the relationship given by the Equation 3.3.

3.2 XFEM Concepts

3.2.1 Level Sets: XFEM

The XFEM is based on the Level Set Method (LSM), a technique used to describe a strong or weak discontinuity and track its behavior. For our case, we are working with strong discontinuities (a crack). We use a scalar-based function within a surface domain whose zero-level is considered as a discontinuity. As a consequence, the surface is subdivided into two subdomains Γ^+ and Γ^- and depending the location of the discontinuity the Level Set Function is considered positive or negative. This method has been very attractive because it works wonders with XFEM, allowing to model the crack growth without remeshing. A level set method is the set of all points at which the function attains a specified value. This technique is very useful to represent surfaces in problems where we need to track the interface. In principle, two functions Φ and Ψ are used to describe the crack location fully. If we set the level set $\Phi = 0$, this will represent the crack face. The intersection of level sets $\Psi = 0$ and $\Phi = 0$ denotes the crack front. The functions are defined by all nodal values, and the spatial variation is determined by the classical finite element (FE) shape functions. The function values only need to be specified at the nodes belonging to elements divided by the crack.

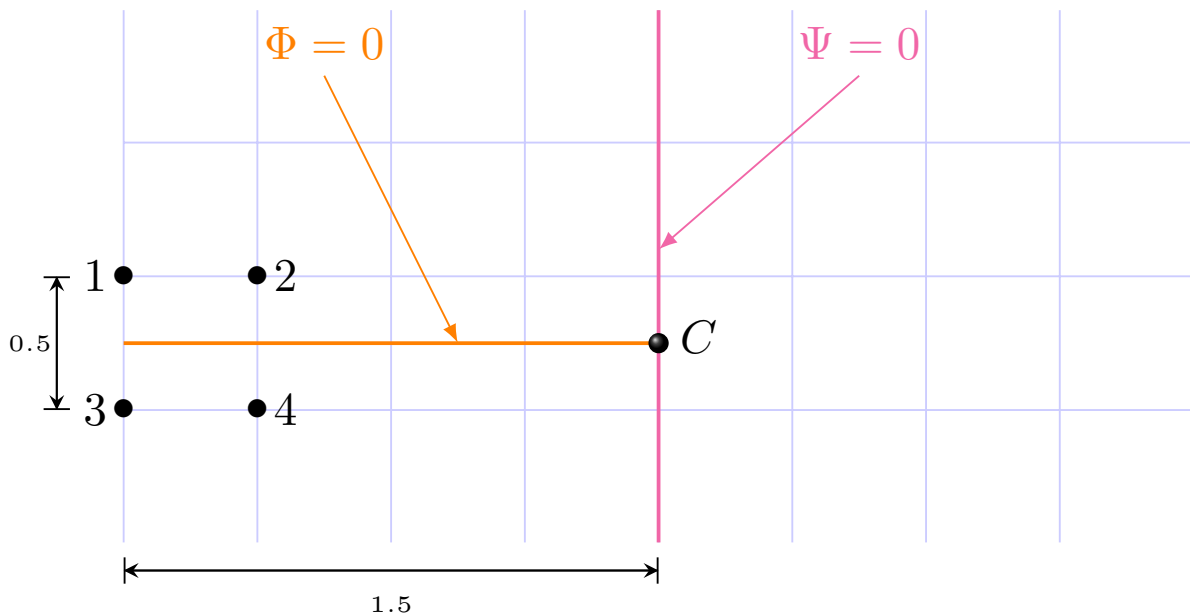


Figure 3.3: CalculatingSignDistance

Figure 3.3 shows that the nodal value of the function Φ is the node distance from the crack face. The function will have a positive value on one side of the crack face, and negative on the other. The Level Set Functions share a common aspect with FEM; the functions are defined to finite locations in the domain using $\phi_i = \phi(x_i)$ and using the standard interpolation element shape functions they are interpolated to know the desired values at the element interiors by:

$$\phi^h(x) = \sum_i N_i(x) \cdot \phi_i \quad (3.7)$$

The nodal value of the function Ψ is the signed distance of the node from an almost-orthogonal surface passing through the crack front. The function Ψ has zero value on this surface and is negative on the side towards the crack. On Table 3.2.1 we can see that for nodes 1 through 4 all signed distances values are related to the reference to the crack front and crack face.

Node	Φ	Ψ
1	+ 0.25	-1.5
2	+ 0.25	-1.0
3	- 0.25	-1.5
4	- 0.25	-1.0

Table 3.1: Calculation of Φ and Ψ

The signed distance shown in Figure 3.4 is a level set function that is described by:

$$\phi(x) = \pm \min_{\forall x \in \Gamma} \|x - x_\Gamma\|, \forall x \in \Omega \quad (3.8)$$

where the sign varies according to the location from positive to negative. The value $\|\cdot\|$ represents the Euclidean Norm that is defined as:

$$\|z\| = \sqrt{z_1^2 + z_2^2 + z_3^2 + \dots + z_n^2} \quad (3.9)$$

The crack tip and Heaviside enrichment functions are multiplied by the conventional shape functions. Hence, the enrichment is local around the crack. The crack is located using the level set method. Heaviside function accounts for displacements jumps across the crack according to Equations 3.10.

$$H(\underline{X}) = \begin{cases} +1 & \text{for } (\underline{X} - \underline{X}^*) \cdot \underline{n} \geq 0 \\ -1 & \text{for } (\underline{X} - \underline{X}^*) \cdot \underline{n} < 0 \end{cases} \quad (3.10)$$

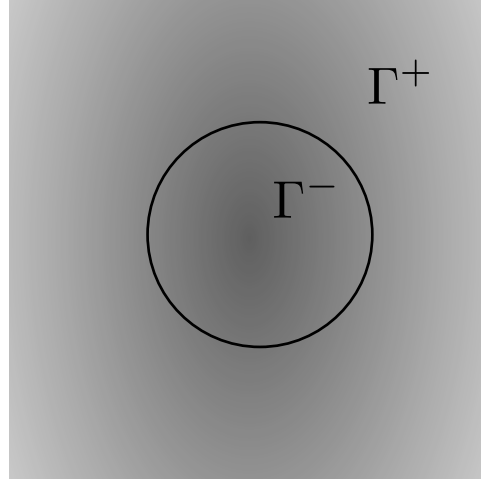


Figure 3.4: Signed Distance

Now, considering a discontinuity in an arbitrary domain located at a point x in a finite element model, the displacements can approximate at the selected point according to Belytschko and Black (1999) as follows:

$$u^h(x) = u^{FE} + u^{enr} = \sum_{j=1}^n N_j(x) u_j + \sum_{k=1}^m N_k(x) \xi(x) a_k \quad (3.11)$$

The term u_j denotes the standard degrees of freedom in a classical FEM approach while a_k is a set of degrees of freedom added to the standard finite element model. The value of $\xi(x)$ denote the enrichment functions (additional functions) affected by the discontinuity. The previous value can be chosen depending the type of enrichment desired which is dominated by the type of discontinuity or singularity. For an example, if a crack tip enrichment is desired the Heaviside function can be used and the formulation becomes:

$$u^h(x) = \sum_{I \in N} N_I(x) u_I + H(x) a_I + \sum_{\alpha=1}^4 F_{\alpha}(x) b_I^{\alpha} \quad (3.12)$$

where $H(x)$ represents the Heaviside function, a_I the nodal enrichment of DOF, and the last term of the function represents the crack tip enrichment.

3.2.2 XFEM Element Formulation

Since XFEM is mesh independent, we used the same discretized problem from previous section. However, we are going to apply a strong discontinuity (crack) to the second spring element. In this context, a Heaviside enrichment function will be applied. The standard displacements are denoted by the variable u . The enrichment is applied to the nodes that belongs to the element that contains the crack (element 2: nodes 2 and 3) denoted by the dashed line as seen in Figure 3.5. Therefore, the element two now has four degrees of freedom, two standard degrees of freedom and two enriched degrees of freedom; the whole structure now hold a total amount of six degrees of freedom (four standard and two enriched nodes).

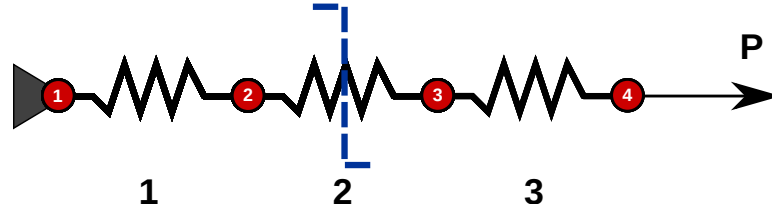


Figure 3.5: One-dimensional Set Spring Elements with a crack in the second element

The stiffness matrix for the XFEM element is given by

$$K_{XFEM} = \begin{bmatrix} K_{uu} & K_{ud} \\ K_{du} & K_{dd} \end{bmatrix} \quad (3.13)$$

each component in the matrix is

$$\begin{aligned} K_{uu} &= \int_0^L (B_{std}^u)^T D B_{std}^u dx \\ K_{ud} &= \int_0^L (B_{std}^u)^T D B_{enr}^d dx \\ K_{du} &= \int_0^L (B_{std}^d)^T D B_{enr}^u dx \\ K_{dd} &= \int_0^L (B_{enr}^d)^T D B_{enr}^d dx \end{aligned} \quad (3.14)$$

Element No.1

The enrichment function $H(x) = +1$ the standard shape functions are develop with the enrichment accordingly

$$H(\underline{X}) = \begin{cases} +1 & \text{for } (\underline{X} - \underline{X}^*) \cdot \underline{n} \geq 0 \\ -1 & \text{for } (\underline{X} - \underline{X}^*) \cdot \underline{n} < 0 \end{cases} \quad (3.15)$$

$$\begin{aligned} N_{std}^u &= \left[1 - \frac{x}{L} \quad \frac{x}{L} \right] \\ N_{enr}^d &= H \left[\frac{x}{L} \right] \\ B_{std}^u &= \left[-\frac{1}{L} \quad \frac{1}{L} \right] \\ B_{enr}^d &= H \left[\frac{1}{L} \right] \end{aligned} \quad (3.16)$$

Substituting the values of 3.16 into Equation 3.14 we have

$$\begin{aligned} K_{uu} &= \int_0^L (B_{std}^u)^T D B_{std}^u dx = \frac{EA}{L} \begin{bmatrix} 1 & -1 \\ -1 & 1 \end{bmatrix} \\ K_{ud} &= \int_0^L (B_{std}^u)^T D B_{enr}^d dx = \frac{EA}{L} \begin{bmatrix} -1 \\ 1 \end{bmatrix} \\ K_{du} &= \int_0^L (B_{std}^d)^T D B_{enr}^u dx = \frac{EA}{L} \begin{bmatrix} -1 \\ 1 \end{bmatrix} \\ K_{dd} &= \int_0^L (B_{enr}^d)^T D B_{enr}^d dx = \frac{EA}{L} \end{aligned} \quad (3.17)$$

$$K_{\text{Element1}} = \frac{EA}{L} \begin{bmatrix} 1 & -1 & -1 \\ -1 & 1 & 1 \\ -1 & 1 & 1 \end{bmatrix} \quad (3.18)$$

Enrichment Function for Element No.2

The element number 2 is cut completely by the crack. Here the Heaviside Function is applied to both nodes with the following enrichment

$$H(\underline{X}) = \begin{cases} +1 & \text{for } (\underline{X} - \underline{X}^*) \cdot \underline{n} \geq 0 \\ -1 & \text{for } (\underline{X} - \underline{X}^*) \cdot \underline{n} < 0 \end{cases} \quad (3.19)$$

$$\begin{aligned} N_{std}^u &= \left[1 - \frac{x}{L} \quad \frac{x}{L} \right] \\ N_{enr}^d &= H \left[1 - \frac{x}{L} \quad \frac{x}{L} \right] \\ B_{std}^u &= \left[\frac{-1}{L} \quad \frac{1}{L} \right] \\ B_{enr}^d &= H \left[\frac{-1}{L} \quad \frac{x}{L} \right] \end{aligned} \quad (3.20)$$

$$K_{uu} = EA \int_0^L (B_{std}^u)^T B_{std}^u dx = \frac{EA}{L} \begin{bmatrix} 1 & -1 \\ -1 & 1 \end{bmatrix} \quad (3.21)$$

The discontinuity requires individual integration due to the separation given by the crack. The integration is performed in the left and in the right of the cut at element 2 by Γ^- and Γ^+ . The advantage of this partition is that no extra degrees of freedom are added to the model.

Integration on Γ^+ Is carried out, here the Heaviside function $H(x) = +1$

$$K_{uu}^+ = EA \int_0^{\frac{L}{2}} (B_{std}^u)^T B_{enr}^d dx = \frac{EA}{2L} \begin{bmatrix} 1 & -1 \\ -1 & 1 \end{bmatrix} \quad (3.22)$$

$$K_{dd}^+ = EA \int_0^{\frac{L}{2}} (B_{enr}^d)^T B_{enr}^d dx = \frac{EA}{2L} \begin{bmatrix} 1 & -1 \\ -1 & 1 \end{bmatrix} \quad (3.23)$$

Integration on Γ^- Is carried out, here the Heaviside function $H(x) = -1$

$$K_{ud}^- = EA \int_{\frac{L}{2}}^L (B_{std}^u)^T B_{enr}^d dx = \frac{EA}{2L} \begin{bmatrix} 1 & -1 \\ -1 & 1 \end{bmatrix} \quad (3.24)$$

$$K_{aa}^- = EA \int_{\frac{L}{2}}^L (B_{enr}^d)^T B_{enr}^d dx = \frac{EA}{2L} \begin{bmatrix} 1 & -1 \\ -1 & 1 \end{bmatrix} \quad (3.25)$$

After independent integration, the results must be combined together

$$K_{ud} = \frac{EA}{2L} \begin{bmatrix} 1-1 & -1+1 \\ -1+1 & 1-1 \end{bmatrix} = \frac{EA}{2L} \begin{bmatrix} 0 & 0 \\ 0 & 0 \end{bmatrix} \quad (3.26)$$

$$K_{dd} = \frac{EA}{2L} \begin{bmatrix} 1+1 & -1-1 \\ -1-1 & 1+1 \end{bmatrix} = \frac{EA}{L} \begin{bmatrix} 0 & 0 \\ 0 & 0 \end{bmatrix} \quad (3.27)$$

The user must remember that by symmetry the value $K_{du} = K_{ud}^T$.

The stiffness matrix for element 2 becomes

$$K_{\text{Element2}} = \frac{EA}{L} \begin{bmatrix} 1 & -1 & 0 & 0 \\ -1 & 1 & 0 & 0 \\ 0 & 0 & 1 & -1 \\ 0 & 0 & -1 & 1 \end{bmatrix} \quad (3.28)$$

Element No. 3

The enrichment type for the last element becomes $H(x) = -1$

$$\begin{aligned} N_{std}^u &= \left[1 - \frac{x}{L} \quad \frac{x}{L} \right] \\ N_{enr}^d &= H \left[1 - \frac{x}{L} \right] \\ B_{std}^u &= \left[\frac{-1}{L} \quad \frac{1}{L} \right] \\ B_{enr}^d &= H \left[\frac{-1}{L} \right] = \left[\frac{x}{L} \right] \end{aligned} \quad (3.29)$$

$$\begin{aligned}
K_{uu} &= \int_0^L (B_{std}^u)^T B_{std}^u dx = \frac{EA}{L} \begin{bmatrix} 1 & -1 \\ -1 & 1 \end{bmatrix} \\
K_{ud} &= \int_0^L (B_{std}^u)^T B_{enr}^d dx = \frac{EA}{L} \begin{bmatrix} -1 \\ 1 \end{bmatrix} \\
K_{du} &= \int_0^L (B_{std}^d)^T B_{enr}^u dx = \frac{EA}{L} \begin{bmatrix} -1 \\ 1 \end{bmatrix} \\
K_{dd} &= \int_0^L (B_{enr}^d)^T B_{enr}^d dx = \frac{EA}{L}
\end{aligned} \tag{3.30}$$

$$K_{\text{Element3}} = \frac{EA}{L} \begin{bmatrix} 1 & -1 & -1 \\ -1 & 1 & 1 \\ -1 & 1 & 1 \end{bmatrix} \tag{3.31}$$

The global stiffness matrix can be assembled together using connectivity numbers and connectivity vectors as

$$K_G = \begin{bmatrix} 1 & -1 & 0 & 0 & -1 & 0 \\ -1 & 2 & -1 & 0 & 1 & 0 \\ 0 & -1 & 2 & -1 & 0 & -1 \\ 0 & 0 & -1 & 1 & 0 & 1 \\ -1 & 1 & 0 & 0 & 2 & -1 \\ 0 & 0 & -1 & 1 & -1 & 2 \end{bmatrix} \tag{3.32}$$

After applying the boundary conditions we have to solve the following system

$$\begin{bmatrix} 2 & -1 & 1 & 0 \\ -1 & 2 & 0 & -1 \\ 1 & 0 & 2 & -1 \\ 0 & -1 & -1 & 2 \end{bmatrix} \begin{Bmatrix} u_2 \\ u_3 \\ \theta_1 \\ \theta_2 \end{Bmatrix} = \begin{Bmatrix} 0 \\ P \\ 0 \\ -P \end{Bmatrix} \tag{3.33}$$

An the displacements are found as

$$\begin{pmatrix} u_1 \\ u_2 \\ u_3 \\ u_4 \\ \theta_1 \\ \theta_2 \end{pmatrix} = \begin{pmatrix} 0 \\ \frac{P}{2} \\ \frac{P}{2} \\ P \\ -\frac{P}{2} \\ -\frac{P}{2} \end{pmatrix} \quad (3.34)$$

The enriched XFEM with Cohesive behavior can be approximated as

$$u(x) = N_i(x) u_i + H(x) N_j(x) \theta_j \quad (3.35)$$

The displacements are calculated as

$$u(x_1) = u_1 = 0 \quad (3.36)$$

$$u(x_2) = u_2 + H(x_2) \theta_1 = \frac{P}{2} - \frac{P}{2} = 0 \quad (3.37)$$

$$u(x_3) = u_3 + H(x_3) \theta_2 = \frac{P}{2} - \frac{P}{2} = P \quad (3.38)$$

$$u(x_4) = u_3 = P \quad (3.39)$$

The results of the XFEM approach can be seen on Figure 3.6. The results shows the main attractive feature of XFEM, a discontinuity located within the element number 2.

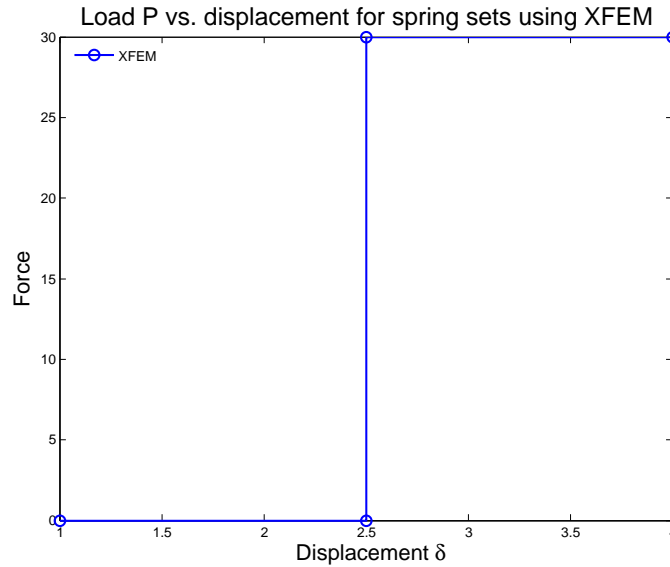


Figure 3.6: 1D Set Spring Elements with Crack at second element using XFEM

3.3 Cohesive Zone Model

3.3.1 Triangular Traction Separation Law

The incorporation of the one-dimensional (1D) element causes a strong discontinuity. The material degradation is modeled using a Triangular CZM law. Sometime this law is referred as a bilinear law. The bilinear cohesive zone law reflects damage in the form of traction separations. For this reason, a step function is used as the only enrichment function for the stiffness of the element. In general, the equation can be written as,

However, Equation 3.49 comes from assuming that the material behavior at the discontinuous point is from the phenomenological law shown in Figure 3.7. The construction of our cohesive law is simple but effective. The energy required to cause delamination is shaded in Figure 3.7 and is defined as follows:

$$G_{IC} = \frac{1}{2} T_{ult} \delta \quad (3.40)$$

where T_{ult} represents the maximum cohesive strength that the material will resist before losing its stability and $\delta = \delta_f - \delta_0$. The value of G_{IC} refers to delamination energy parameter. This quantity can be measured experimentally in the laboratory. The parameter T_{ult} is the cohesive

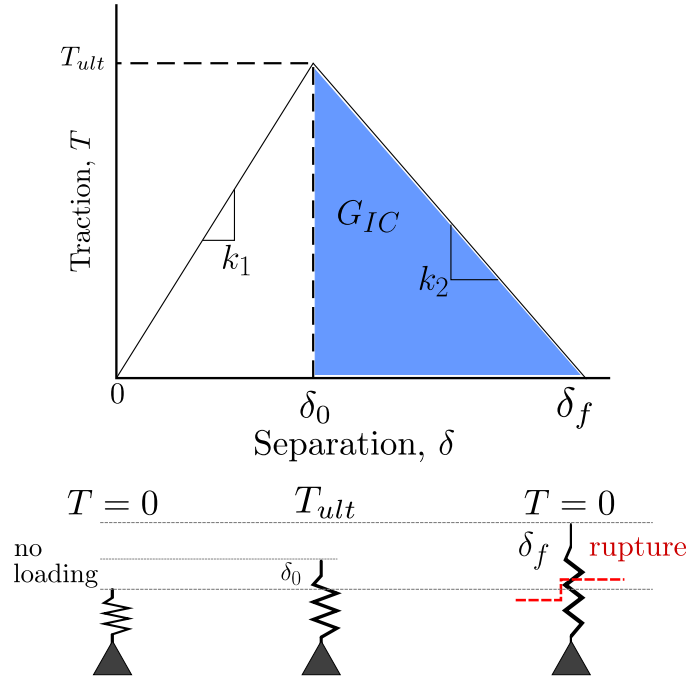


Figure 3.7: Triangular Traction Separation Law

strength that can be measured in several ways according to ASTM. Initially, there is no loading applied to the interface, that means a zero separation and a zero traction is applied. If the spring is stretched, it will achieved a maximum traction T_{ult} , there is a linear behavior between zero and δ_0 with a proportion ok k_1 . After the maximum traction is attained a separation δ_0 is reached, that means a permanent damage to the spring element. After this point the element stiffness is going to decay with a stiffness k_2 until a maximum allowed spring length is achieved and rupture takes place. At this point the element release all the energy and it doesn't exist anymore. The traction separation law is defined as

$$T = k_1 \delta_0 \quad (3.41)$$

The value of k_1 is called reduce stiffness but also is known as a penalty stiffness and is equivalent to

$$k_1 = \frac{1}{2} T_{ult} \quad (3.42)$$

This value corresponds to the slope of the triangular region located between 0 and δ_0 . The unloading region is characterize by the same behavior but traction becomes is related with the value $(\delta_f - \delta_0)$ which represents the base of the second triangular region. For this particular

work, the material properties are considered as linear elastic, and the constitutive relationship is then expressed as

$$\sigma = D\varepsilon \quad (3.43)$$

where D represents the elastic modulus tensor, and for a 1D element $D = EA$. Assuming small displacements, the stress-strain relationship is given by

$$\varepsilon = \nabla^s u \quad (3.44)$$

3.3.2 Exponential Traction Separation Law

The Triangular Law is linear and easy to implement. However, computationally speaking we have to deal with the discontinuity at δ_c . One way to overcome this problem is to use softening laws or an exponential law. Here, we discuss an exponential constitutive laws for single bond rupture based on interfacial damage mechanics approach (Goyal 2002). Let us assume the two material points between the upper and lower surfaces, which are coincident when unstretched, are given by a nonlinear spring. Now, we express the traction-separation law as follows:

$$T(\delta) = \delta \frac{T_c}{\delta_c} \exp \left[\frac{1 - \left(\frac{\delta}{\delta_c} \right)^\beta}{\beta} \right] \quad (3.45)$$

where δ is the opening, T_c the maximum force of the spring that occurs at the critical δ_c . The parameter β is a positive real number and defines whether the rupture is brittle or ductile: a high value models brittle fracture, and a low value models ductile fracture. For our application, we use a high β to model the adhesive, which acts brittle-like. In this context, we can express the total energy release rate as follows:

$$G_c = \int_0^\infty T(\delta) d\delta = T_c \delta_c \Psi(\beta) \quad (3.46)$$

where $\Psi(\beta)$ is “correction” factor that takes into account the brittle or ductile nature of the fracture and it is defined as

$$\Psi(\beta) = \left\{ \beta^{\frac{2-\beta}{\beta}} \Gamma \left[\frac{2}{\beta} \right] \exp \left[\frac{1}{\beta} \right] \right\} \quad (3.47)$$

where $\Gamma[z]$ is the Euler gamma function of argument z . Note that $\Psi(\beta)$ does not have an upper bound but it does have lower bound. We can show that as the material behaves as a perfectly brittle material ($\beta \rightarrow \infty$) the value leads to 1/2, which leads to

$$G_c = \int_0^\infty T(\delta) d\delta = T_c \delta_c \frac{1}{2} \quad (3.48)$$

The same value obtained for the triangular model! Goyal (2002) showed that using $\beta = 5.2$, we can compare to the triangular model, and it will be the value we use in this work.

3.4 Cohesive Element Method

3.4.1 Cohesive Element

Consider the the same discretization of the previous, however, the element number two as described by the cohesive spring at the center. The cohesive spring located at the center must be interpreted as a cohesive force, not a new element. The spring was used for illustration purposes only.



Figure 3.8: 1D Set Spring Elements with Cohesive Crack using XFEM

$$\begin{bmatrix} \int_{\Omega} (B_{std}^u)^{T\sigma} D \nabla^s u^h \\ \int_{\Omega} (B_{enr}^T) D \nabla^s u^h + \int_{\Gamma_{coh}} (N_{enr}^a)^T k \mathbb{U}(u^h) \end{bmatrix} = \begin{bmatrix} \int_{\Gamma} (N_{std}^u)^{T_i} \\ \int_{\Gamma} (N_{enr}^a)^{T_i} \end{bmatrix} \quad (3.49)$$

Element No. 1

The same procedure for XFEM is applied for element one in this section. The local stiffness matrix remains the same.

Element No. 2

The same procedure for XFEM is applied for element one in this section. The local stiffness matrix remains the same, but with the inclusion of the cohesive force the element stiffness matrix becomes

$$K_{\text{element2}} = \begin{bmatrix} \frac{EA}{L} & -\frac{EA}{L} & 0 & 0 \\ -\frac{EA}{L} & \frac{EA}{L} & 0 & 0 \\ 0 & 0 & \frac{EA}{L} + k & -\frac{EA}{L} + k \\ 0 & 0 & -\frac{EA}{L} + k & \frac{EA}{L} + k \end{bmatrix} \quad (3.50)$$

Element No. 3

The same procedure for XFEM is applied for element one in this section. The local stiffness matrix remains the same.

Simplifying, the global stiffness matrix becomes

$$K_{\text{Element3}} = \begin{bmatrix} \frac{EA}{L} & -\frac{EA}{L} & 0 & 0 & -\frac{EA}{L} & 0 \\ -\frac{EA}{L} & \frac{2EA}{L} & -\frac{EA}{L} & 0 & \frac{EA}{L} & 0 \\ 0 & -\frac{EA}{L} & \frac{2EA}{L} & -\frac{EA}{L} & 0 & -\frac{EA}{L} \\ 0 & 0 & -\frac{EA}{L} & \frac{EA}{L} & 0 & \frac{EA}{L} \\ -\frac{EA}{L} & \frac{EA}{L} & 0 & 0 & \frac{2EA}{L} + k & -\frac{2EA}{L} + k \\ 0 & 0 & -\frac{EA}{L} & \frac{EA}{L} & -\frac{EA}{L} + k & \frac{2EA}{L} + k \end{bmatrix} \begin{Bmatrix} u_1 \\ u_2 \\ u_3 \\ u_4 \\ \theta_1 \\ \theta_2 \end{Bmatrix} = \begin{Bmatrix} 0 \\ 0 \\ 0 \\ P \\ 0 \\ 0 \end{Bmatrix} \quad (3.51)$$

The displacements

$$\begin{Bmatrix} u_1 \\ u_2 \\ u_3 \\ u_4 \\ \theta_1 \\ \theta_2 \end{Bmatrix} = \begin{Bmatrix} 0 \\ 4.6667 \\ 8.6667 \\ 13.3333 \\ -0.6667 \\ -0.6667 \end{Bmatrix} \quad (3.52)$$

For the problem, the displacements can be found if we assume $\frac{EA}{L} = 1$, $k = 3$ and $P = 4$ and applying the boundary conditions we can get the values of the unknowns

$$u(x_1) = u_1 = 0 \quad (3.53)$$

$$u(x_2) = u_2 + H(x_2) \theta_1 = 4.6667 - 0.66667 = 4 \quad (3.54)$$

$$u(x_3) = u_3 + H(x_3) \theta_2 = 8.6667 + (-1)(-0.6667) = 9.333 \quad (3.55)$$

$$u(x_4) = u_4 = 13.333 \quad (3.56)$$

Figure 3.9 shows the discontinuity for cohesive behavior located at center of element 2

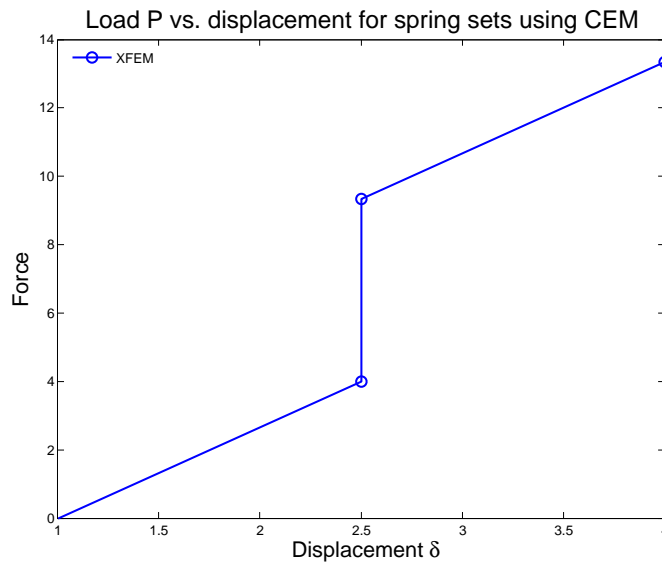


Figure 3.9: Cohesive Element Method

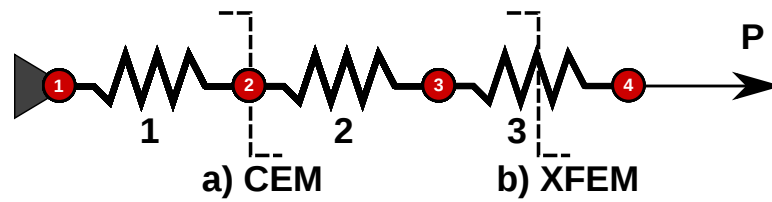


Figure 3.10: Combined CE and XFEM

3.4.2 Combined CE and XFEM

Figure 3.10 shows our implementation that combines CE and XFEM together. If the spring element fails at a node, case a) is activated and cohesive element approach is used. Now, if the crack cuts within the element, case b) is activated and the XFEM algorithm is used.

3.5 ABAQUS Capabilities

ABAQUS is a software with several FEA modules well known for its high performance and quality. It is used for the most challenging simulations among the industry and academic community. The software features several analysis modules that are divided mainly into two groups: ABAQUS/Standard and ABAQUS/Explicit.

3.5.1 ABAQUS/Standard and ABAQUS/Explicit

The ABAQUS/Standard analysis is for general purpose as it can be used for a wide spectrum of problems related to structural/mechanical, thermal, vibration, buckling analyzes, crack propagation and so on. Also, this module is well suited for implicit integration problems such as static, low-speed dynamic events and steady-state transport analyzes. ABAQUS/Standard provides an automatic solution incrementation steps. The rate of convergence is monitored to determine whether appropriate time (load) increments are applied or not and for linear problems the method is stable when the stiffness $[K]$ is linear. The increment size is increased if only a few iterations are required, but decreased if convergence is slow. Now, if convergence cannot be obtained during the analysis, the increment size is decreased automatically, and further attempts are made. The implicit procedure of ABAQUS/Standard is cost-effective when the problem under study can be solved using relatively few load increments. This module uses Newton's Method to solve for static equilibrium problems.

The iterations are repeated in each increment until convergence is achieved, which has the following implications: force equilibrium is achieved at every node, moment equilibrium is attained at every node, displacements corrections are small compared to incremental displacements. However, the reader must bear in mind that Newton's Method has a finite radius of convergence. If a large increment is used, then a solution cannot be obtained because the initial state lies outside of the radius equilibrium state. Thus, there is a restriction on the increment size.

On the other hand, ABAQUS/Explicit is designed to simulate short transient dynamic events such as an automotive crashworthiness or a ballistic impact. This module is characterized for handling non-linear behavior related to slow crushing and contact behavior. Furthermore, the Explicit procedure is well-suited for high-speed (wave propagation) applications. The explicit procedure performs the analysis using a technique that made use of a large number of inexpensive, small, time(load) increments.

3.5.2 Overview of ABAQUS Implementation

Although ABAQUS has become a powerful FE code, the challenge is when it does not have the module we are looking for. It always seems tempting to develop our own FE code using Object Oriented Languages such as *FORTRAN*, *C++* and *Python*. This might solve the problem initially, but we are challenged when we need to solve complex problems that need complex solvers. Not to mention that the user will need to implement complex solution schemes at expenses of code overhead (non-optimized code) for all the FEA basic procedures: pre-processing, processing, post-processing and data manipulation.

ABAQUS/Standard and ABAQUS/Explicit are contained in a unique environment illustrated in Fig. 3.11 called ABAQUS/CAE (ABAQUS Complete Environment). This graphical ecosystem provides a rich modeling, pre-processing and post-processing analysis product. ABAQUS/CAE takes advantages of CAD models with advanced meshing techniques, resulting in a coherent graphical user interface (GUI). ABAQUS/Standard has an interface, is the User Subroutine UEL, that allows every user the creation of user defined elements. In this work, we use in ABAQUS/STANDARD /CAE.

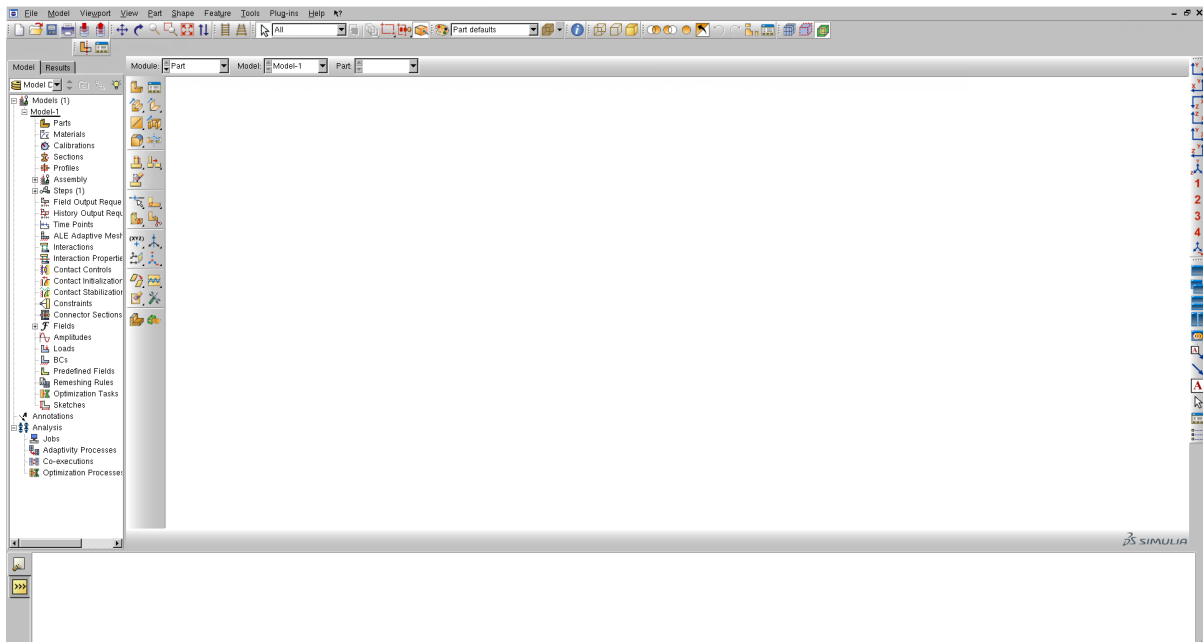


Figure 3.11: ABAQUS/CAE Graphical User Interface

3.6 Implementing the Triangular Element

ABAQUS® allows advanced tasks such as *Users Elements* (UEL) that are not available in the ABAQUS® default element libraries. ABAQUS/Standard provides all users to use user-defined subroutines (UEL) to create elements that are not available by default in the element library. These elements can be used in combination with other ABAQUS elements and can be used for most of the applications available in ABAQUS /Standard. If the user creates more than one element using the UEL routine, all element definition must reside on a single subroutine file, each one with its properties and characteristics. The UEL definition can be used as a traditional finite element that represent a geometric part of a structure or can be used as an artificial system that applies forces at one location of a model depending on displacements at some other parts of the model. This way we can implement the Triangular Element.

3.6.1 Writing a User Element (UEL)

The heading for the UEL in ABAQUS is given by the following heading (in FORTRAN 77):

```

SUBROUTINE UEL (RHS , AMATRX , SVARS , ENERGY , NDOFEL ,
1 NRHS , NSVARS , PROPS , NPROPS , COORDS , MCRD , NNODE , U , DU , V ,
2 A , JTYPE , TIME , DTIME , KSTEP , KINC , JELEM , PARAMS , NDLOAD ,
3 JDLTYP , ADLMAG , PREDEF , NPREDEF , LFLAGS , MLVARX , DDLMAG ,
4 MDLOAD , PNEWDT , JPROPS , NJPROP , PERIOD)
C Must Include the following to communicate with ABAQUS
  INCLUDE 'ABA\_PARAM.INC'
C Second part of the subroutine heading
  DIMENSION RHS (MLVARX , * ) , AMATRX (NDOFEL , NDOFEL ) , SVARS ( * ) ,
1 PROPS ( * ) , ENERGY ( 7 ) , COORDS (MCRD , NNODE ) , U (NDOFEL ) ,
2 DU (MLVARX , * ) , V (NDOFEL ) , A (NDOFEL ) , TIME ( 2 ) , PARAMS ( * ) ,
3 JDLTYP (MDLOAD , * ) , ADLMAG (MDLOAD , * ) , DDLMAG (MDLOAD , * ) ,
4 PREDEF ( 2 , NPREDEF , NNODE ) , LFLAG ( 4 ) , JPROPS ( * )
C From this point goes the user programming

```

The UEL interface has specific requirements to define the user-defined element to the model. For an example, in stress analysis the user must include in the code a definition for stiffness, and in heat transfer the corresponding variable to code for conductivity. ABAQUS

is responsible for the management of the UEL by calling the routine every time information about of the user element is needed. Also, ABAQUS provides the values of nodal variables at the end of the increment: initial coordinates, velocities, total displacements and the values of solution-dependent state variables at the beginning of the increment. Now, depending on the usage the routine must define several variables:

1. The contribution of the element to the stiffness matrix or Jacobian.
2. The contribution of the element to the residual vector.
3. The updated values of the solution dependent variables at the end of the increment.

By design, ABAQUS will call the subroutine twice during every iteration and updates all variables and provides all values to the routine at the correct time. For stress analysis, ABAQUS will respond to the increment as shown in Fig. 3.12. For step 1, the value of $\{u\}^n$ is extrapo-

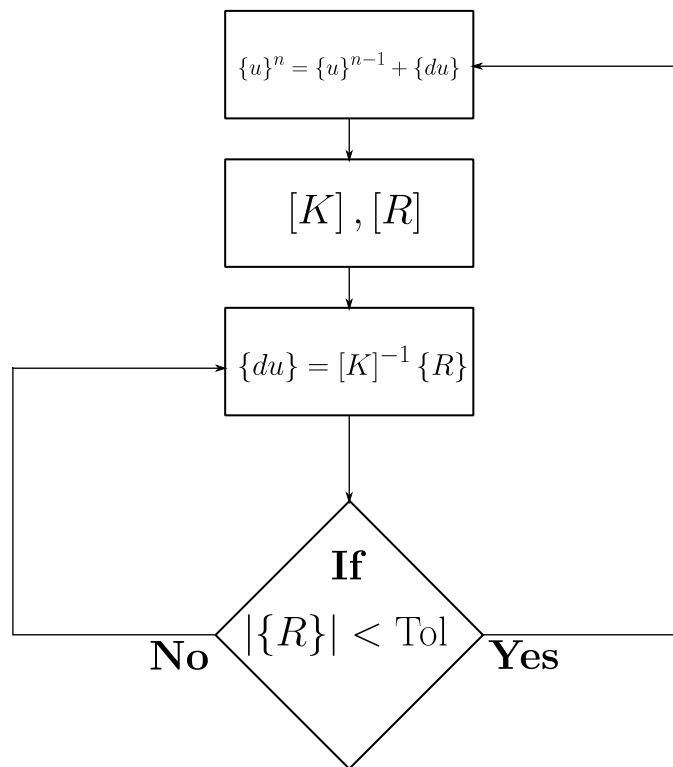


Figure 3.12: ABAQUS/Standard Increment Flow

lated from the previous increment. Then, for step 2, it is given a value of $\{u\}^n$, calculating then

the stiffness matrix $[K]$ and the residual vector $[R]$. Then, ABAQUS will solve for $\{du\}$. If $|\{R\}| < \text{Tolerance}$ the algorithm goes to step 1, else it goes to step 3 which is the next iteration.

Several important parameters must be specified by the user while using creating the sub-routine. These parameters are used to calculate the stresses and displacement. However, if the user is interested in other quantities, he has the option available to him. The definable variables are:

1. **COORDS** : This is an array in which the user stores the coordinate values of the element in use.
2. **U** : This array contains the total values of all variables.
3. **PROPS** : This can be defined as an array that stores the values of Material Properties or Geometrical properties.

Now, an important part is defining the stiffness matrix that is given by the required parameter **AMATRX**. The residual vector contribution must return to ABAQUS® into the **AMATRX** and the contribution to the right hand side vector **RHS**.

3.6.2 Stiffness Matrix

A fundamental equilibrium equation can be written as

$$[K] \{U\} = \{F\} \quad (3.57)$$

where K is the stiffness matrix, U the displacement vector, and F the load vector. When using the UEL interface, the routine must define K in the global coordinate system. This requirement involves the usage of the transformation of K from local coordinates (x,y) to global (X,Y) coordinates. Using the Eq. 3.57, the residual vector can be rewritten as

$$[K] \{U\} - \{F\} = \{R\} \quad (3.58)$$

where $\{R\}$ is the residual vector. If the equation is solved exactly, the residual vector becomes zero. However, sometimes round-off errors arise during the solution, or inaccuracies arise due to the non-linearity nature of the problem. As a consequence, the residual vector cannot always be zero. ABAQUS convergence criteria is based on the magnitude of that residual, being an very important definition to be coded. The contribution for the stress problem of the user

element to the residual vector is calculated as

$$\{R\} = -[K]\{U\} . \quad (3.59)$$

3.6.3 ABAQUS Input File

In ABAQUS, the user has the option to build a complete Finite Element Model by simply using a text editor of his preference. This script file is called the input file, and its extension ends with `.inp` to be recognized as a valid ABAQUS input command. An example of an input file can be located at the Appendix B. The Systèmes (2012) and Simulia (2014) include in detail the meaning and usage of all ABAQUS keywords. Rather than a computer language, ABAQUS keywords form options blocks or group cards with flags that form a compilation of statements that form data blocks relevant to the FEM. Every option block is formed at the beginning of each line with a keyword, and if the block requires additional data input, these can be written below the keyword line. For example the following part of an input file includes the information of our current implementation:

```
*ELEMENT, TYPE=U1001, ELSET=USER
    1, 101, 102
    2, 102, 103
    3, 103, 104
```

All ABAQUS keywords begin with an asterisk (*), and are followed by the block name. For this particular example, the block name starts with the keyword **ELEMENT** which invokes the creation of an element, a fundamental part in the creation of the mesh. Due to the variety of elements available, is necessary to specify which type will be used for the model with a unique name. Our UEL element is identified on the subroutine as **TYPE=U1001**. The reader must have in mind that ABAQUS® does not allow to rename the element as the user wants, is required that every user element name must start with the letter **U** followed by a number that must be less than **9999**. The UEL is stored in an element set called **ELSET** that must be called **USER**. This allows better manipulation of the element depending on what is desired by the user. In the example above, the first element contains the node numbers **101** and **102** and the second element contains the node numbers **102** and **103**, this methodology is very powerful and convenient because the analyst can make references to the **RTRUSS** set when defining other option blocks.

```
** *****  
**      Begin User Element  
** *****  
*USER ELEMENT, TYPE=U1001, NODES=2, COORDINATES=1,  
PROPERTIES=4, VARIABLES=10
```

Here the degrees of freedom are defined, according to the element formulation and four properties are defined with six desired variables for the output (e.g. σ_{11} , σ_{22} , σ_{33} , σ_{12} , σ_{13} , U).

When using UEL, ABAQUS[®] does not support element visualization. The user is responsible for the calculation of stresses and other quantities desired. The reason is that ABAQUS[®] viewer is not aware of the element formulation and shape functions. Therefore, this limitation restricts us to use other external monitoring tools such as MATLAB to investigate and validate the results at the points of interest.

The force and displacement history are plotted in MATLAB. This quantity is one of the most important values in experimental work involving DCB because it characterizes the bonded structure and provides information on Mode I, G_{IC} . This test consists of rectangular adherents bonded along their length with a region free of adhesive extended in some way into the joint.

3.7 Validation

The following example illustrates the use of ABAQUS to predict in a DCB layered specimens. Cohesive Zone Model combined with XFEM Heaviside functions, a triangular traction separation law, and crack initiation was used for this purpose. In order to validate the models, we plan to use the published experimental work by Davies (2002), Robinson and Song (1992) and Song et al. Song et al. (2008).

The model with cohesive elements is analyzed in ABAQUS/Standard using the subroutine UEL and uses a damaged linear elastic constitutive model. The model with CZ criterion and XFEM is also analyzed to predict debonding for the quasi-static test. Also, a hypothetical model for a 2D plate is provided. Figure 3.14 is an augmented view of the mesh created for the DCB models. The first two benchmarks (Davies 2002) share similar geometrical properties with the exception of the last benchmark (Song et al. 2008).

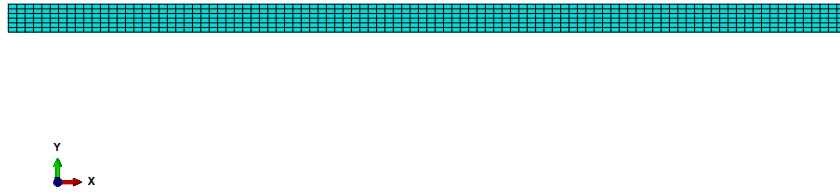


Figure 3.13: Finite Element

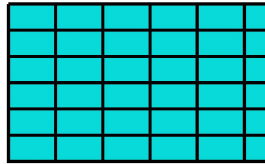
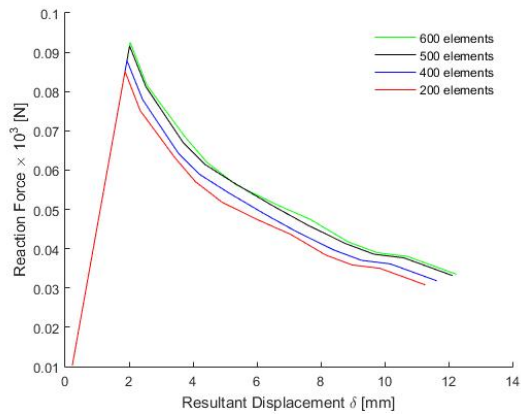


Figure 3.14: Augmented Finite Element Mesh

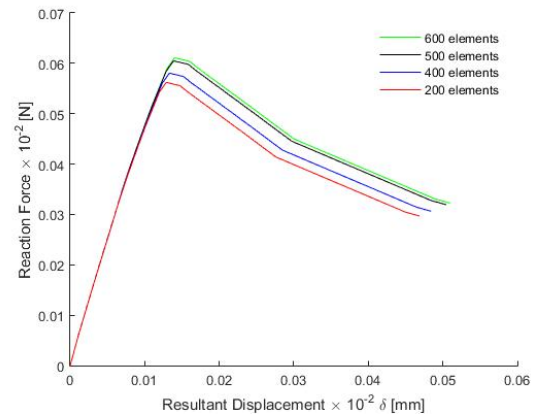
3.7.1 Optimal Mesh and Tolerance

Since this work is concentrated on the determination of the load displacement behavior for the DCB model, similar meshes were selected for all benchmarks. Figure 3.15 illustrates the best mesh required for all models. As the amount of elements is incremented at the bond line, the optimal mesh appears to converge around 600 elements. The reader must have in mind that all benchmarks share similar geometrical dimensions, hence the convergence must be almost the same. It can be seen clearly that the shape for the curves is preserved and the maximum loads are predicted very close to one another. Since the implemented custom element is a linear spring-like element, a better response for convergence can be seen for small deflections as seen in 3.15(c) in contrast with Figures 3.15(a) and 3.15(b).

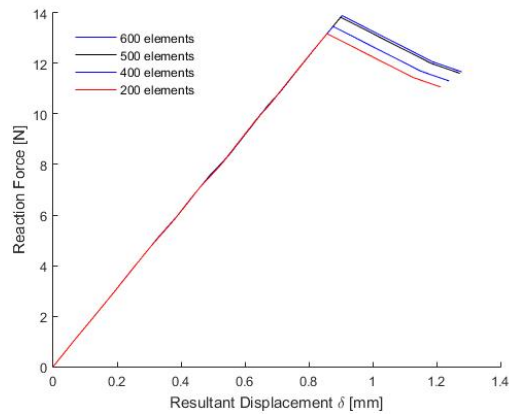
The optimal tolerance is performed for the models for the optimum mesh of 600 elements. As we can see in Figure 3.16 the optimal value of 1×10^{-5} is found as the ideal tolerance number used as a parameter to decide when the material is going to present degradation due to a maximum traction load. When the critical value of $(\delta_0 - \delta) \leq 1 \times 10^{-5}$ is achieved, the damage on the model takes place. After that point material degradation is present on the springs until a displacement failure δ_f is obtained. The Figures 3.16(a), 3.16(b) and 3.16(c) reflect no sensitivity to the selected tolerance for the value of δ selected for our models.



(a) Convergence Benchmark 1

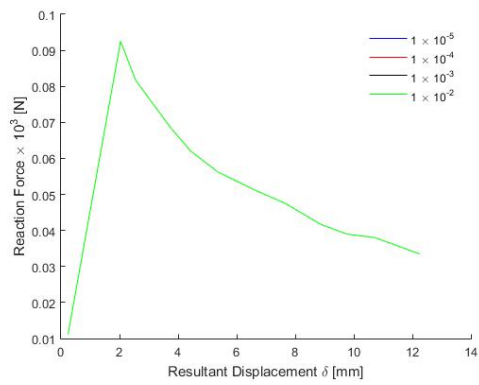


(b) Convergence Benchmark 2

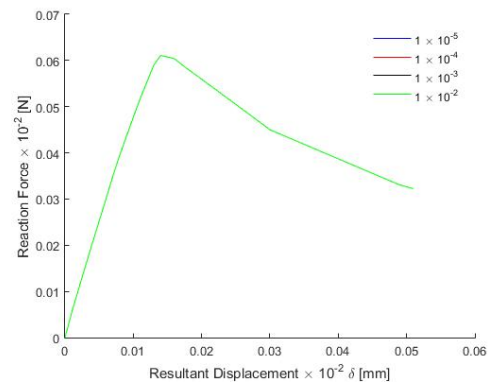


(c) Convergence Benchmark 3

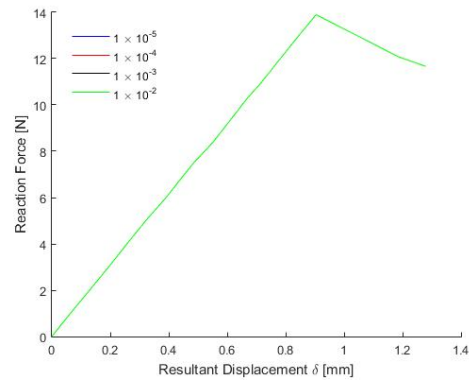
Figure 3.15: Mesh Convergence.



(a) Tolerance Benchmark 1



(b) Tolerance Benchmark 2



(c) Tolerance Benchmark 3

Figure 3.16: Optimal Tolerance

3.7.2 Experimental Setup

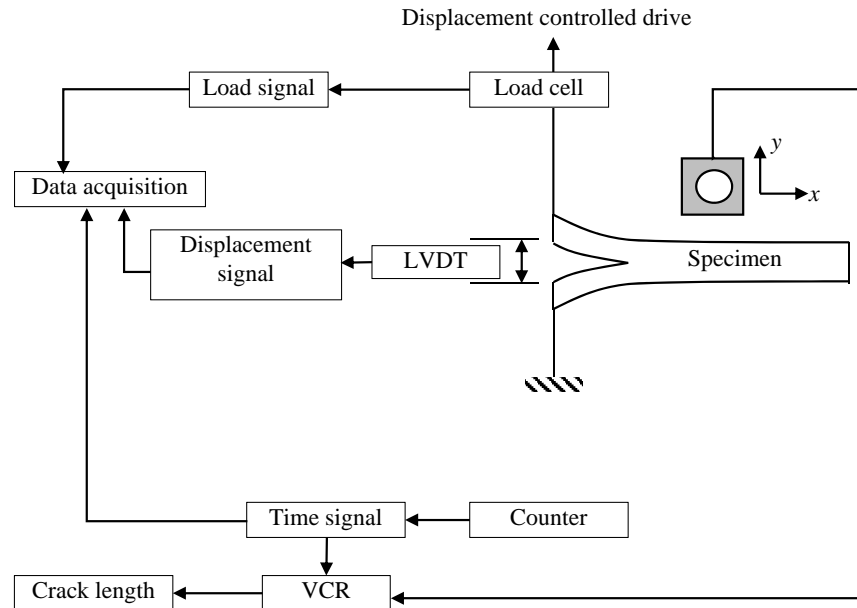


Figure 3.17: Experimental Setup picture for DCB by Robinson (1992)

An example of the experimental setup is provided for clarification purposes. The experimental setup shown in Figure 3.17 was performed by Robinson (1992) using a tensile test machine with a controlled displacement rate. During the experiment the load P and the cross head displacement δ was recorded by a computer that at the same time records a marking signal that indicates crack progression through typical increments of 5 mm. A linear variable differential transformer (LVDT) is located at the tip of the DCB to measure the linear displacement δ . Also when delamination is propagated, the crack front is monitored using a video camera and recorded with a VCR. The conventional DCB tests were performed using a load rate of 5 mm/min in order to perform a quasi-static test.

3.7.3 Benchmark 1: Analytical Solution

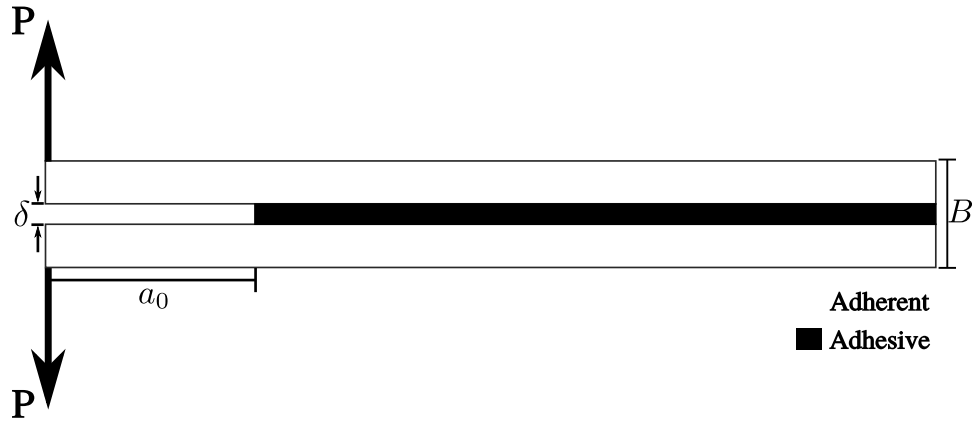


Figure 3.18: Double Cantilever Beam Specimen

The material properties for the unidirectional laminate lay-up Benchmark 1 are:

$$E_{xx} = 126 \text{ GPa}, \quad E_{yy} = 7.5 \text{ GPa}, \quad G_{xy} = 4.981 \text{ GPa}, \quad \nu_{xx} = \nu_{yz} = \nu_{xz} = 0.263$$

Delamination Properties: $G_{IC} = 0.281 \text{ N/mm}$, damage initiation stress = 57 MPa. This benchmark uses a 2D simplification of the DCB model as shown on Figure 3.18 and the test involves Mode I Fracture Toughness, built with $(+45, -45, 0, 90)_{ns}$ plies. This kind of test is the standard used to measure the values of G_{IC} . The testbed assumes an initial straight crack a_0 . Based on Davies (2002), wide edge effects (B) are ignored. For this reason, Davies (2002) determined that using a simple beam theory is appropriate. From basic mechanics the deflection of a cantilever beam is given by the simple expression

$$y = \frac{P}{6EI}(-x^3 + 3L^2x - 2L^3) \quad (3.60)$$

The deflection at the tip is obtained by letting $x = 0$ and taking as a positive frame of reference the vertical direction the equation becomes

$$y = \frac{PL^3}{3EI} \quad (3.61)$$

Now, let y equal to $\Delta/2$ and L equal to the crack length a , this is because the analysis is applied to one half of the DCB. The reader must take in understand that classical elemental beam theory does not take into consideration large rotations at the tip of the DCB model. It

is assumed that all displacements are perfectly oriented towards the vertical direction and the load is perfectly applied at the free edge end of the DBC. The displacement Δ due to the two applied opposite forces at each leg P is given by

$$\frac{\Delta}{2} = \frac{Pa^3}{3EI} \quad (3.62)$$

where EI is flexural rigidity and a the crack length. According to Equation 3.62, the work done can be calculated when the crack extends a finite distance δ_a .

$$W = P \delta\Delta = P \frac{2Pa^2}{EI} \delta_a \quad (3.63)$$

Energy is consumed during this process, and this relates the strain energy release rate G_{IC} . The crack propagation is achieved if

$$\frac{2Pa^2}{EI} \delta a = G_{IC} 2B \delta_a \quad (3.64)$$

The material employed is carbon epoxy T800/924 with the properties indicated by Robinson and Song (1992).

3.7.4 Benchmark 1: Numerical Simulation

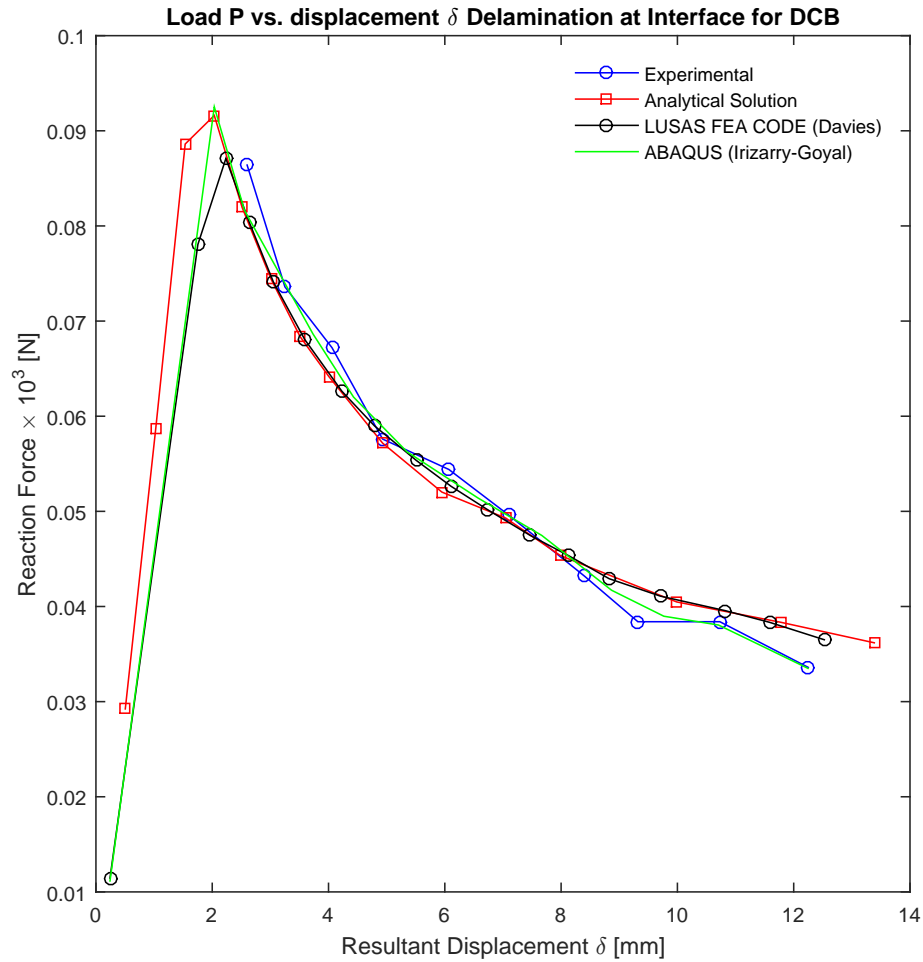


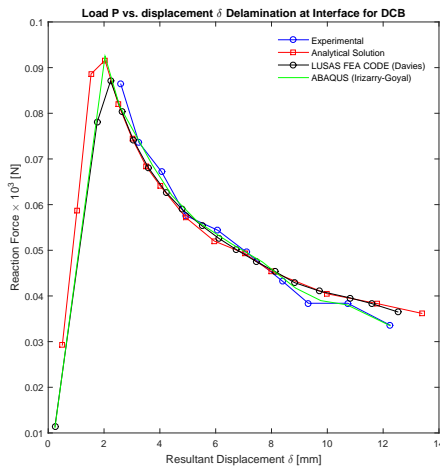
Figure 3.19: Load P vs. displacement δ - Delamination at Interface for DCB

The material properties for the unidirectional 20 prepreg layers Benchmark 2 are:

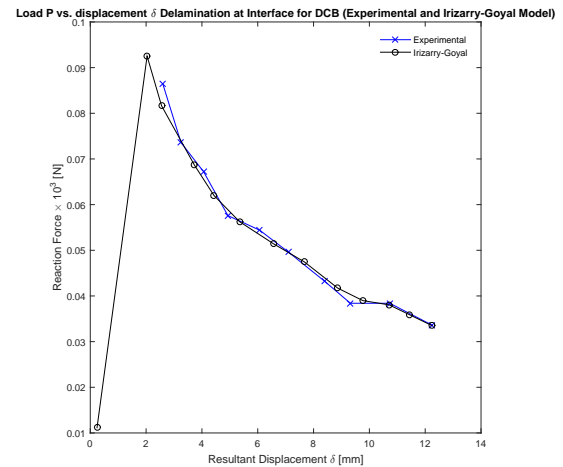
$$E_1 = 120\text{GPa}, E_2 = 7.8\text{GPa}, G_{12} = 3.25\text{GPa}, \nu_{12} = 0.32$$

Delamination Properties: $G_{IC} = 1200 \text{ J/m}^2$, damage initiation stress = 57 MPa. Davis (2002)

performed numerical simulations and compared the values with experimental data, closed-form solution, and the LUSAS FEA code, as shown in Figure 3.19. As we can see the experimental value does not start close to the origin. This is because a data acquisition machine with sensors has been used. The machine is only aware of the change of the crack length δ , thus an offset is present. The closed-form solution adopts a conservative change of crack length less than 1 mm in order to cover the most of the spectrum of the resultant displacement. On the other hand, the LUSAS code assumes a small δ and achieve a maximum peak close to the analytical solution. After unloading (after the maximum peak), each plot correlates well with the behavior of the displacement.



(a) Double Cantilever Beam Joint



(b) Single Lap Joint

Figure 3.20: Benchmarks Comparison

Figure 3.20 shows a comparison of Triangular Model to the ones presented by Davies (2002). Figure 3.20(a) shows the experimental data presented by Davies (2002) and the proposed model. Compared to the closed-form solution, we can observe that our model suffers a shift on the linear part between 0 and 2 mm. However at the maximum peak, our model can capture the maximum value of the analytical solution. In contrast, the LUSAS code under predicts the maximum peak value given by the close form solution. In contrast, the slightly overpredicts the maximum value but correlates better in comparison with LUSAS code. In terms of the softening region, implementation shows a maximum difference of 8%.

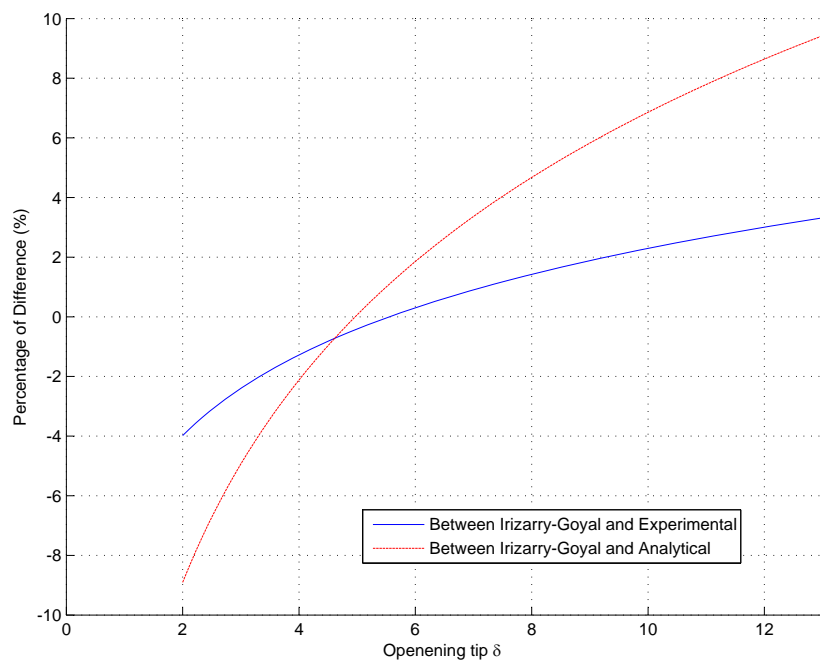


Figure 3.21: Error for Benchmark 1

3.7.5 Benchmark 2: Numerical Simulation Using Loading Blocks

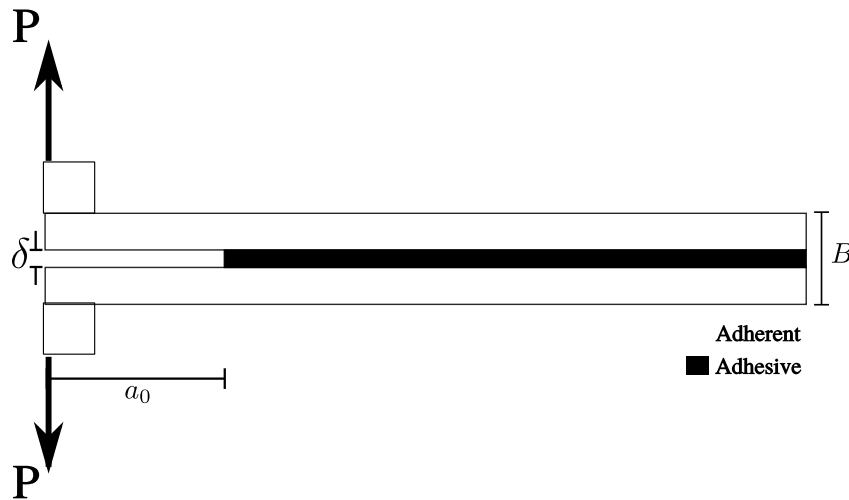


Figure 3.22: Double Cantilever Beam Specimen with loading blocks

The material properties for the unidirectional 20 prepeg layers Benchmark 2 are:

$$E_1 = 120\text{GPa}, E_2 = 7.8\text{GPa}, G_{12} = 3.25\text{GPa}, \nu_{12} = 0.32$$

Figure 3.23 shows the results obtained with the Triangular Model. We plot it against the theoretical and experimental values obtained by Davies (2002). This experiment is almost identical to the previous (Benchmark 1). However, the experimental delamination on the DCB specimen was imposed by loading blocks. The reader should take into consideration that including loading blocks into the simulation reflects a boundary condition that is closer to the real experiment. Large deformations take place during the experiment. The theoretical model achieved a maximum peak value between 0.001 and 0.02×10^{-2} mm, after the peak value the curve shows a smooth behavior. The experimental data shows a shift approximately by 0.05×10^{-2} mm if we compared with the theory.

The Triangular Model shows an excellent correlation with the experimental values on the linear part of the curve. The linear part experiments a 3% of difference compared with the experimental data. However, the maximum peak values is not achieved by the Triangular Model, there is a 10% of difference with respect the experimental data from the peak value to the final resultant displacement. These results indicate that a progressive delamination can be considered accurate within the linear part of the Reaction vs. Resultant Displacement plot. Beyond that point, discrepancies exist in the range of 10% – 12% of difference, but the shape of the behavior of the curve is preserved. Since the Triangular Model uses a linear approach

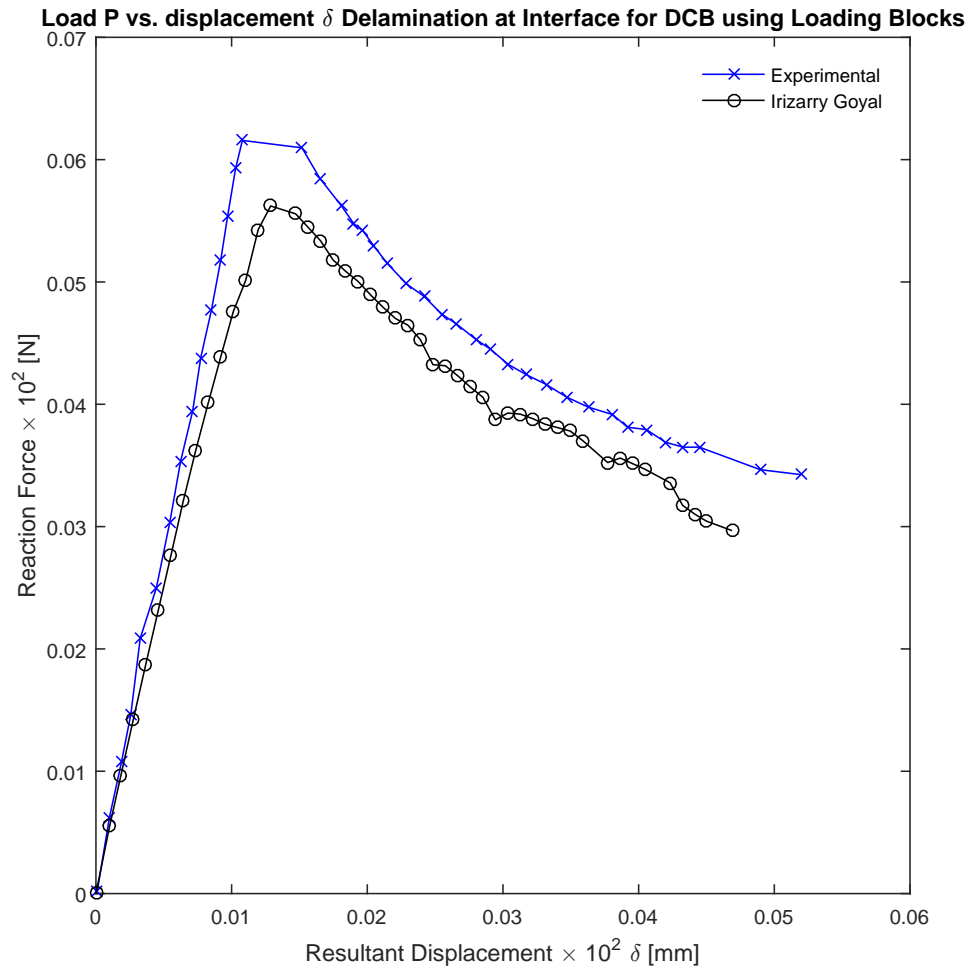


Figure 3.23: Load P vs. displacement δ - Delamination at Interface for DCB with loading blocks

that tries to capture a nonlinear behavior, these types of results are expected. However, further improve will be the basis for future research.

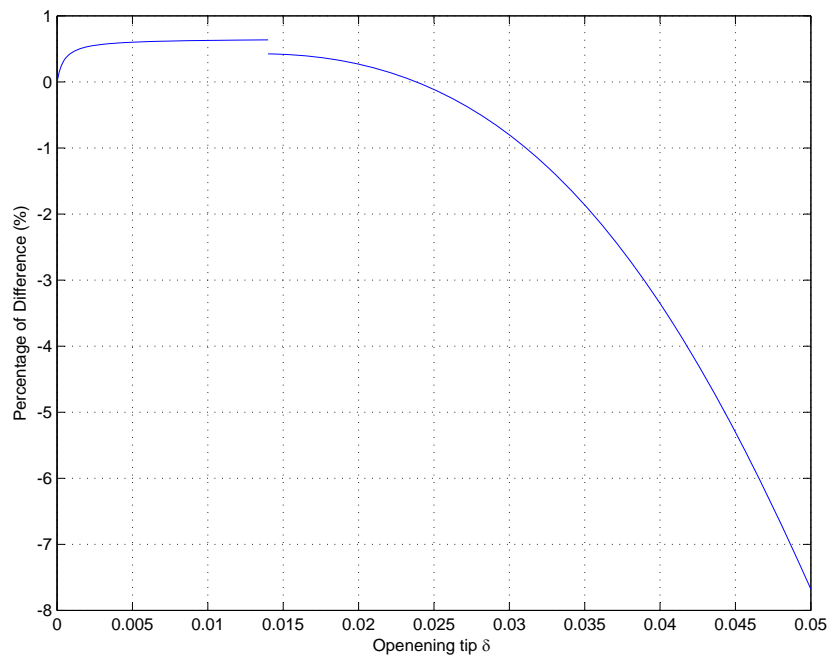


Figure 3.24: Error for Benchmark 2

3.7.6 Benchmark 3: Standard DCB using Normal Interfacial Strength by Song

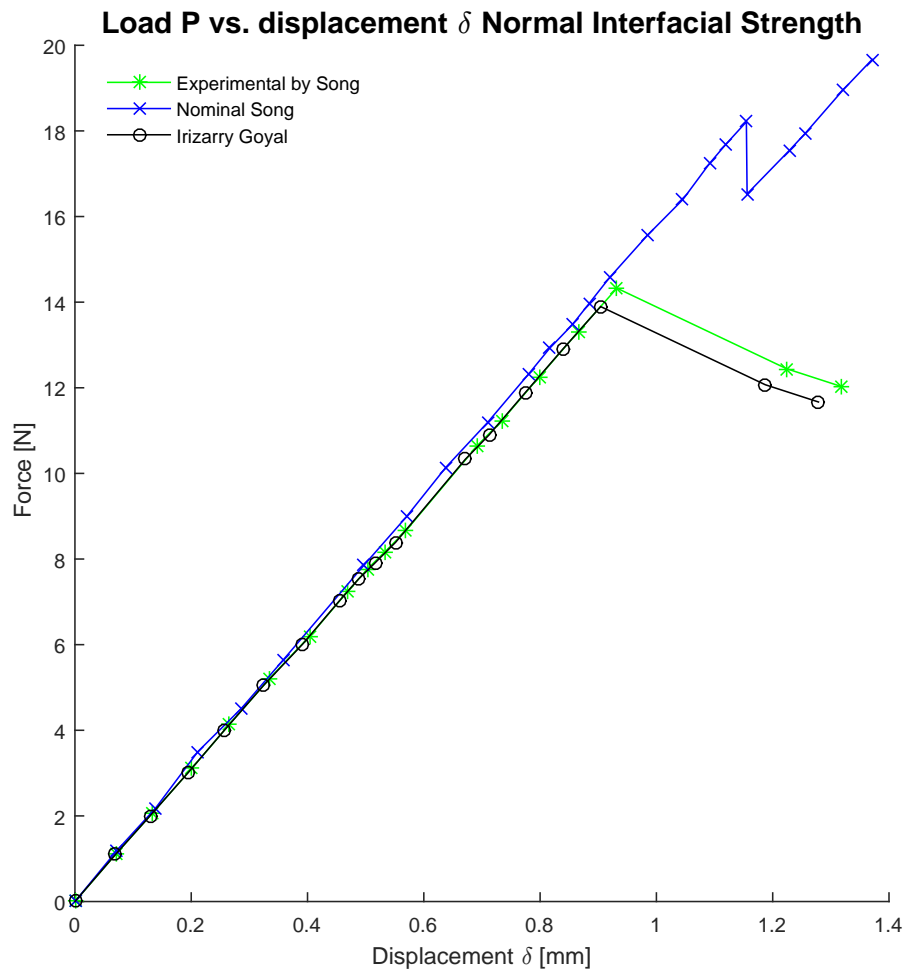


Figure 3.25: Load P vs. displacement δ - Delamination at Interface for DCB with loading blocks

The material properties of AS4/3501-6 for the DCB with stacking sequence $[0_3]$ Benchmark 3 are:

$$E_1 = 148\text{GPa}, E_2 = 10.50\text{GPa}, G_{12} = 5.61\text{GPa}, \nu_{12} = 0.27, G_{IC} = 0.08 \frac{\text{kJ}}{\text{m}^2}$$

The predicted load deflection response is compared with the results of Song et al. (2008) as shown in Figure 3.25. Unlike the previous two benchmarks, this experiment shows small displacements history data. For validation purposes, three different curves are compared. The nominal Strength curve by Song behaves linearly until an approximate value of 1.2 mm is achieved. At this location, a discontinuous value response is obtained. This model over-predicts the strength predicted by the analytical solution. As we can appreciate, the numerical prediction by Song does not follow the softening response of the analytical solution when one Cohesive Zone Element is used. On the other hand the Triangular Model implementation shows a better response on the linear part and at the softening region. For the implementation under predicts the maximum peak to the softening region with a maximum difference of 2% compared to the analytical solution. The predicted load deflection response obtained using the Triangular Model UEL implementation correlates well with the analytical predictions.

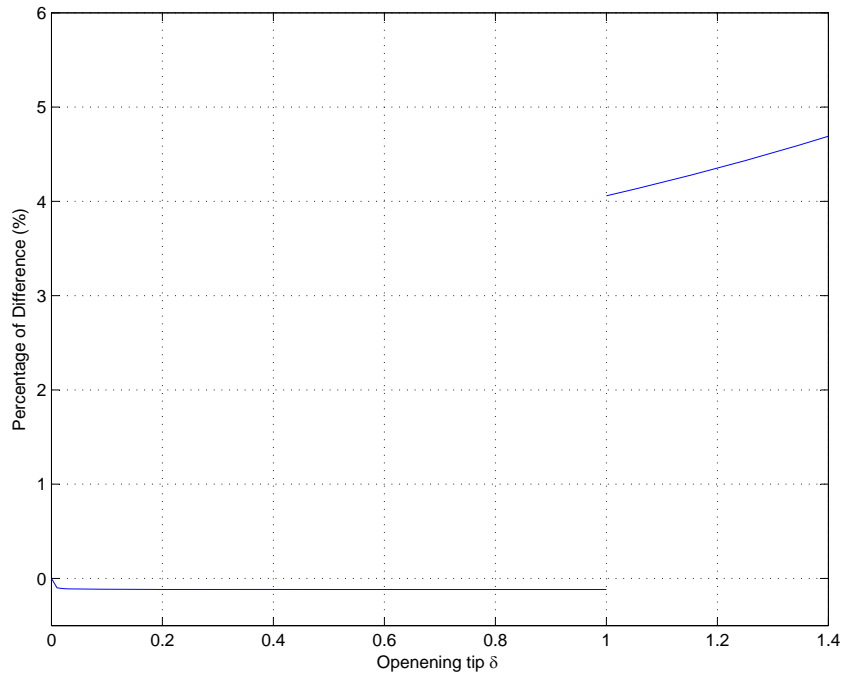


Figure 3.26: Error for Benchmark 3

Chapter 4

Final Remarks

4.1 Conclusion

In the classical FEM, it is necessary to refine the mesh near the crack tip and thus remeshing is a must even after crack propagation. We investigated and developed the Irizarry-Goyal Triangular Mesesodel to predict delamination of the interfacial bonded regions. The model consisted combining the Cohesive Element and Extended Finite Element Methods while using a Triangular traction-separation law.

The model was successfully developed and implemented into ABAQUS via UEL subroutine. The User Element was elaborated using FORTRAN through a customize environment file using Python.

A triangular phenomenological traction law simulates the adhesive behavior while the XFEM technique allows to simulate crack propagation. The interface thickness is under consideration in our model because it is known that adhesive thickness can influence the mechanical properties of the joint. The User Subroutine has been developed within ABAQUS[®] to fit the numerical $P - \delta$ curves defining the constitutive law.

The advantage of the current approach is that a crack propagation path is better simulated due to the discontinuity behavior of the interfacial element when it reaches maximum displacement. In order to verify the performance of the presented combined model, a study of common lap joints has been conducted. Results show that our model is superior when compared to others in the literature.

4.2 Future Work

Most commercial FE software provide interfaces through user subroutines to define material behavior and specialized user elements. The latter cannot be visualized using Abaqus/Viewer or Abaqus/CAE. This is a major drawback because the user element topology is hidden inside the element subroutine, in other words, the software is not aware of what kind of shape functions are being used. Having said that, only elements from the Abaqus element library can be visualized with the Abaqus/Viewer and Abaqus/CAE.

However, ABAQUS® provides certain external rules that allows the user to extract information from the binary databases generated by the software. Therefore as a future work, UEL post-processing is an appropriate way to expand this research. On the other hand, fatigue analysis should be the next step for further development.

Appendix A

ABAQUS® GFROTRAN Environmental File

The following code is the ABAQUS environmental file. Every user customization to the ABAQUS/CAE suite can be include here. This file contains a modification to use the open source GFORTRAN compiler instead of the required Intel Fortran 10.x.x and Intel Fortran 11.x.x .

```
##### abaqus_v6.env file #####

# Modified from standard env file
# Modified by Dr. Vijay Goyal and Emmanuel Irizarry
# Date Modified: August 2015
#
# University of Puerto Rico at Mayaguez
#
# System-Wide Abaqus Environment File
# -----
standard_parallel = ALL
mp_mode = MPI
mp_file_system = (DETECT,DETECT)
mp_num_parallel_ftps = (4, 4)
mp_environment_export = ('MPI_PROPAGATE_TSTP',
'ABA_CM_BUFFERING',
'ABA_CM_BUFFERING_LIMIT',
'ABA_ITERATIVE_SOLVER_VERBOSE',
'ABA_DMP SOLVER_BWDPARALLELOFF',
'ABA_ELP_SURFACE_SPLIT',
'ABA_ELP_SUSPEND',
'ABA_HOME',
'ABA_MEMORY_MODE',
'ABA_MPI_MESSAGE_TRACKING',
```

'ABA_MPI_VERBOSE_LEVEL',
'ABA_PATH',
'ABAQUS_CSE_RELTIMETOLERANCE',
'ABA_RESOURCE_MONITOR',
'ABA_RESOURCE_USEMALLINFO',
'ABAQUS_LANG',
'ABAQUS_CSE_CURRCONFIGMAPPING',
'ABAQUS_MPF_DIAGNOSTIC_LEVEL',
'ABAQUSLM_LICENSE_FILE',
'ABQ_CRTMALLOC',
'ABQ_DATACHECK',
'ABQ_RECOVER',
'ABQ_RESTART',
'ABQ_SPLITFILE',
'ABQ_XPL_WINDOWDUMP',
'ABQ_XPL_PARTITIONSIZE',
'ABQLMHANGLIMIT',
'ABQLMQUEUE',
'ABQLMUSER',
'CCI_RENDEZVOUS',
'DOMAIN',
'DOMAIN_CPUS',
'DOUBLE_PRECISION',
'FLEXLM_DIAGNOSTICS',
'FOR0006',
'FOR0064',
'FOR_IGNORE_EXCEPTIONS',
'FOR_DISABLE_DIAGNOSTIC_DISPLAY',
'LD_PRELOAD',
'MP_NUMBER_OF_THREADS',
'MPC_GANG',
'MPI_FLAGS',
'MPI_FLUSH_FCACHE',
'MPI_RDMA_NENVELOPE',
'MPI_SOCKETBUFSIZE',
'MPI_USE_MALLOPT_MMAP_MAX',
'MPI_USE_MALLOPT_MMAP_THRESHOLD',
'MPI_USE_MALLOPT_SBRK_PROTECTION',

```
'MPI_WORKDIR',
'MPCCI_DEBUG',
'MPCCI_CODEID',
'MPCCI_JOBID',
'MPCCI_NETDEVICE',
'MPCCI_TINFO',
'MPCCI_SERVER',
'MPIEXEC_AFFINITY_TABLE',
'ABAQUS_CCI_DEBUG',
'NCPUS',
'OMP_DYNAMIC',
'OMP_NUM_THREADS',
'OUTDIR',
'PAIDUP',
'PARALLEL_METHOD',
'RAIDDEV_NDREG_LAZYMEM',
'ABA_SYMBOLIC_GENERALCOLLAPSE',
'ABA_SYMBOLIC_GENERAL_MAXCLIQUERANK',
'ABA_ADM_MINIMUMINCREASE',
'ABA_ADM_MINIMUMDECREASE',
'IPATH_NO_CPUAFFINITY',
'MALLOC_MMAP_THRESHOLD',
'ABA_EXT_SIMOUTPUT',
'SMA_WS',
'SMA_PARENT',
'SMA_PLATFORM',
'ABA_PRE_DECOMPOSITION',
'ACML_FAST_MALLOC',
'ACML_FAST_MALLOC_CHUNK_SIZE',
'ACML_FAST_MALLOC_MAX_CHUNKS',
'ACML_FAST_MALLOC_DEBUG',
'MKL_NUM_THREADS',
'MKL_DYNAMIC')
```

```
import driverUtils, os
#-*- mode: python -*-
```

```
#####
#####
# #
# Compile and Link command settings for the Linux 64
  Platform #
# ( AMD Opteron / Intel EM64T ) #
# #
#####
#####

import os, re, glob, driverUtils

#MPI implementation handling
mpiCppl = ''
mp_rsh_command = 'ssh -n -l %U %H %C'
mp_mpi_implementation = PMPI
#mp_mpi_implementation = IMPI #<--- Uncomment this line and
  comment above line to switch to IMPI
if mp_mpi_implementation == PMPI:
pmpipath = driverUtils.locateFile(os.environ.get('ABA_PATH',
  ''), 'pmpi-9.1.2/bin', 'mpirun')
mp_mpirun_path = {PMPI: pmpipath}
mpiCppl = '-DABQ_MPI_PMPI'
if mp_mpi_implementation == IMPI:
impipath = driverUtils.locateFile(os.environ.get('ABA_PATH',
  ''), 'impi-4.1.1/bin', 'mpiexec.hydra')
mp_mpirun_path = {IMPI: impipath}
mpiCppl = '-DABQ_MPI_IMPI'

#fortCmd = "ifort" # <-- Fortran compiler
fortCmd = "gfortran"
cppCmd = "g++" # <-- C++ compiler

# Avoid signal trapping by the Fortran RTE
os.environ["FOR_IGNORE_EXCEPTIONS"] = "1"
# Disable messages from the Fortran RTE
os.environ["FOR_DISABLE_STACK_TRACE"] = "1"
```

```

# Do not let QLogic InfiniPath driver set processor affinity
.
os.environ["IPATH_NO_CPUAFFINITY"] = "1"

# Add the flag "-free" to the compile_fortran command below
  to use free-format FORTRAN 90 syntax.

dirLst = glob.glob('/usr/bin')
if dirLst:
dirLst.sort()
ccDefPath = dirLst[-1] + '/bin'

#compile_fortran = [fortCmd, '-V', '-c', '-fPIC', '-auto', '-
  mP2OPT_hpo_vec_divbyzero=F', '-extend_source', '-fpp', '-
  WB', '-I%i']

compile_fortran = (fortCmd + '_c_fPIC_I%i')

# Additional command-line options for the Intel C/C++
  Compilers:
# '-cxxlib', '-Kc++eh', '-Krtti', '-Kc++', '-pc64', '-
  restrict', '-i-dynamic',
# '-we1011', '-we120', '-we117', '-we556', '-we144', '-we268
  ', '-we1224', '-we167', '-we880'

compile_cpp = [cppCmd,
'-c', '-fPIC', '-w', '-Wno-deprecated', '-DTYPENAME=typename
  ',
'-D_LINUX_SOURCE', '-DABQ_LINUX', '-DABQ_LNX86_64', '-
  DSMA_GNUC',
'-DFOR_TRAIL', '-DHAS_BOOL', '-DASSERT_ENABLED',
'-D_BSD_TYPES', '-D_BSD_SOURCE', '-D_GNU_SOURCE',
'-D_POSIX_SOURCE', '-D_XOPEN_SOURCE_EXTENDED', '-
  D_XOPEN_SOURCE',
'-DHAVE_OPENGL', '-DHKS_OPEN_GL', '-DGL_GLEXT_PROTOTYPES',
'-DMULTI_THREADING_ENABLED', '-D_REENTRANT',
'-DABQ_MPI_SUPPORT', '-DBIT64', '-D_LARGEFILE64_SOURCE', '-
  D_FILE_OFFSET_BITS=64',

```

```

mpiCppImpl,
# '-O0', # <-- Optimization level
# '-g', # <-- Debug symbols
'-I%I']

compile_fmu = [cppCmd,
'-c', '-fPIC', '-I%I']

link_fmu = [cppCmd,
'-fPIC', '-shared', '-o', '%J', '%M']

#link_sl = [fortCmd,
# '-V',
# '-cxxlib', '-fPIC', '-threads', '-shared',
# '%E', '-Wl,-soname,%U', '-o', '%U', '%F', '%A', '%L', '%B',
#   , '-parallel',
# '-Wl,-Bdynamic', '-i-dynamic', '-lifport', '-lifcoremt', '
#   -lmpi']

link_sl = (fortCmd +
"␣-gcc-version=%i␣-fPIC␣-shared␣" +
"%E␣-Wl,-soname,%U␣-o␣%U␣%F␣%A␣%L␣%B␣-Wl,-Bdynamic␣" +
"␣-lifport␣-lifcoremt")

link_exe = [cppCmd,
'-fPIC',
'-Wl,-Bdynamic', '-o', '%J', '%F', '%M', '%L', '%B', '%O', '
-lpthread', '-lm', '-lifcoremt']

# Remove the temporary names from the namespace
del cppCmd
del fortCmd
del mpiCppImpl
if mp_mpi_implementation == PMPI:
del pmpipath
if mp_mpi_implementation == IMPI:
del impipath

```

```
graphicsEnv = driverUtils.locateFile(os.environ['ABA_PATH'],
    'site','graphicsConfig','env')
if graphicsEnv:
    execfile(graphicsEnv)
else:
    raise 'Cannot find the graphics configuration environment
        file(graphicsConfig.env)'

del driverUtils, os, graphicsEnv

del dirLst, ccDefPath

license_server_type=FLEXNET

abaquslm_license_file=""
```

Appendix B

Input File Example

The following code is an example of an Input file with the requirements parameters to include a user subroutine with a load parametrization.

```
*HEADING
BEAM_DIST_LOAD_UEL
*PARAMETER
P =-10.0
*NODE
101,      0.,      0.
102,      10.,     0.
103,      20.,     0.
104,      30.,     0.
105,      40.,     0.
106,      50.,     0.
107,      60.,     0.
108,      70.,     0.
109,      80.,     0.
1010,     90.,     0.
1011,    100.,     0.
** =====
**      Begin User Element
** =====
*USER ELEMENT, TYPE=U1001, NODES=2, COORDINATES=1,
PROPERTIES=4, VARIABLES=10
** NEXT THE FREE DOF ARE DEFINED (Displacement in Y, Rotation in Z)
2,          6
*ELEMENT, TYPE=U1001, ELSET=USER
2,          102,      103
3,          103,      104
4,          104,      105
```

```

5,          105,          106
6,          106,          107
7,          107,          108
8,          108,          109
9,          109,          1010
10,         1010,         1011
*UEL PROPERTY, ELSET=USER
1E6, 108, -10.0, 0.3
** =====
**      Begin B21 Element
** =====
* ELEMENT, TYPE = B21, ELSET=BEAM
1, 101, 102
*BEAM SECTION, SECTION=RECTANGULAR, ELSET=BEAM, MATERIAL=STEEL
6.0, 6.0
*MATERIAL, NAME=STEEL
*DENSITY
7680.,
*ELASTIC
1E6, 0.3
** =====
** Boundary Conditions
** =====
*BOUNDARY
101, ENCASTRE
1011, 2
** =====
**      Loading Condition
** =====
*STEP, NAME=STEP-1, PERTURBATION
*STATIC
*CLOAD
101, 2, <P>
102, 2, <P>
103, 2, <P>
104, 2, <P>
105, 2, <P>
106, 2, <P>

```

```
107, 2, <P>
108, 2, <P>
109, 2, <P>
1010, 2, <P>
1011, 2, <P>
*OUTPUT, FIELD, VARIABLE=PRESELECT
*NODE PRINT
RF, COORD
U, COORD
*EL PRINT
S,
*ENDSTEP
```

Bibliography

- Ahmed, A. (2009). eXtended Finite Element Method (XFEM) - Modeling arbitrary discontinuities and Failure analysis. pp. 196. [Cited on page(s): [20](#)]
- Armentani, E. and R. Citarella (2006). DBEM and FEM analysis on non-linear multiple crack propagation in an aeronautic doubler-skin assembly. *International Journal of Fatigue* 28(5–6), pp. 598–608. [Cited on page(s): [17](#)]
- Babuska, I. and J. M. Melenk (1996). The partition of unity method. *International Journal of Numerical Methods in Engineering* 40, pp. 727–758. [Cited on page(s): [19](#)]
- Belytschko, T. and Black (1999). Elastic crack growth in finite elements with minimal remeshing. *International Journal for Numerical Methods in Engineering* 45(5), pp. 601–620. [Cited on page(s): [19](#), [28](#)]
- Benzley, S. E. (1974). Representation of Singularities with Isoparametric Finite Elements. *International Journal for Numerical Methods in Engineering* 8(3), pp. 537–545. [Cited on page(s): [19](#)]
- Bialstrokecki, R. A., Z. Ostrowski, A. J. Kassab, Q. Yin, and E. Sciubba (2002). Coupling BEM, FEM and analytic solutions in steady-state potential problems. *Engineering Analysis with Boundary Elements* 26(7), 597–611. [Cited on page(s): [17](#)]
- Blal, N., L. Daridon, Y. Monerie, and S. Pagano (2011). Criteria on the artificial compliance inherent to the intrinsic cohesive zone. *Comptes Rendus Mécanique* 339(12), 789–795. [Cited on page(s): [22](#)]
- Bordas, S. and B. Moran (2006). Enriched finite elements and level sets for damage tolerance assessment of complex structures. *Engineering Fracture Mechanics* 73(9), pp. 1176–1201. [Cited on page(s): [19](#)]
- Camanho, P. P., C. G. Dávila, and S. T. Pinho (2004). Fracture analysis of composite co-cured structural joints using decohesion elements. *Fatigue & Fracture of Engineering Materials & Structures* 27(9), 745–757. [Cited on page(s): [22](#)]
- Chahine, E., P. Laborde, and Y. Renard (2011). A non-conformal eXtended Finite Element approach: Integral matching XFEM. *Applied Numerical Mathematics* 61(3), pp. 322–343. [Cited on page(s): [19](#)]

- Chen, E., L. Lawson, and M. Meshii (1995). The effect of fatigue microcracks on rapid catastrophic failure in Al-SiC composites. *Materials Science and Engineering: A* 200(1), 192–206. [Cited on page(s): 20]
- Chessa, J., P. Smolinski, and T. Belytschko (2002). The extended finite element method (XFEM) for solidification problems. *International Journal for Numerical Methods in Engineering* 53(8), pp. 1959–1977. [Cited on page(s): 20]
- Combescure, A., A. Gravouil, D. GrÃl'goire, and J. Rethore (2008). XFEM a good candidate for energy conservation in simulation of brittle dynamic crack propagation. *Computer Methods in Applied Mechanics and Engineering* 197(5), pp. 309–318. [Cited on page(s): 20]
- Crocombe, A., I. Ashcroft, and M. Wahab (2008). Environmental degradation. pp. pp. 225–241. [Cited on page(s): 11]
- Davies, G. (2002). Benchmarks For Composite Delamination. pp. pp.1–39. [Cited on page(s): 10, 48, 53, 55, 56, 58]
- Dolbow, J., N. Moes, and T. Belytschko (2001). An extended finite element method for modeling crack growth with frictional contact. *Computer Methods in Applied Mechanics and Engineering* 190(51-52), pp. 6825–6846. [Cited on page(s): 22]
- Dolbow, N., J. Dolbow, and T. Belytschko (1999). A finite element method for crack growth without remeshing. *Int. J. Numer. Meth. Engng* 46, pp. 131–150. [Cited on page(s): 18]
- E., H. C. and S. M. J. J. James H. Starnes (2001). *An Assessment of the State-of-the-Art in the Design and Manufacturing of Large Composite Structures for Aerospace Vehicles*. Technical Report. [Cited on page(s): 22]
- Geubelle, P. H. and J. S. Baylor (1998). Impact-induced delamination of composites: a 2D simulation. *Composites Part B: Engineering* 29(5), pp. 589–601. [Cited on page(s): 22]
- Goyal, V. K. (2002). *Analytical Modeling of the Mechanics of Nucleation and Growth of Cracks*. Ph. D. thesis, Virginia Tech, Aerospace and Ocean Engineering Department. [Cited on page(s): 37, 38]
- GrÃl'goire, D., H. Maigre, J. Rethore, and A. Combescure (2007). Dynamic crack propagation under mixed-mode loading-Comparison between experiments and X-FEM simulations. *International Journal of Solids and Structures* 44(20), pp. 6517–6534. [Cited on page(s): 20]
- Griffith, A. A. (1921). The phenomena of rupture and flow in solids. *Philosophical Transactions of the Royal Society of London. Series A, containing papers of a mathematical or physical character*, pp. 163–198. [Cited on page(s): 11, 15]

- Irwin, G. (1956). Onset of Fast Crack Propagation in High Strength Steel and Aluminum Alloys. *Sagamore Research Conference Proceedings 2*, pp. 289–305. [Cited on page(s): 11]
- Kaiyuan, L., L. Shuyao, and L. Guangyao (2006). A simple and less-costly meshless local Petrov-Galerkin (MLPG) method for the dynamic fracture problem. *Engineering analysis with boundary elements* 30(1), pp. 72–76. [Cited on page(s): 11]
- Kettil, P., J. RÅsdenas, C. Aguilera Torres, and N.-E. Wiberg (2007). Strength and deformation of arbitrary beam sections using adaptive FEM. *Computers & Structures* 85(1–2), pp. 15–29. [Cited on page(s): 17]
- Konuk, I., , and S. Yu (2010). A cohesive element framework for dynamic ice-structure interaction problems–Part III: Implementation. In *Proceedings of the 29th International Conference on Ocean, Offshore and Arctic Engineering*. [Cited on page(s): 21]
- Konuk, I., A. Gurtner, , and S. Yu (2009). A cohesive element framework for dynamic ice-structure interaction problems–Part II: Implementation. In *Proceedings of the 28th International Conference on Ocean, Offshore and Arctic Engineering, Honolulu, Hawaii, USA*. [Cited on page(s): 21]
- Liu, C. and J. Nairn (1999). Analytical and experimental methods for a fracture mechanics interpretation of the microbond test including the effects of friction and thermal stresses. *International Journal of Adhesion and Adhesives* 19(1), pp. 59–70. [Cited on page(s): 13]
- Liu, Y. and S. Mahadevan (2007). Threshold stress intensity factor and crack growth rate prediction under mixed-mode loading. *Engineering Fracture Mechanics* 74(3), pp. 332–345. [Cited on page(s): 17]
- Log, R., M. Beringhier, Y. Chastel, L. Delannay, et al. (2007). Reducing computational cost and allowing automatic remeshing in FEM models of metal forming coupled with polycrystal plasticity. [Cited on page(s): 19]
- Lu, W., R. Lubbad, S. Lset, and K. HylandG (2012). Cohesive zone method based simulations of ice wedge bending: a comparative study of element erosion, cem, dem and xfem. In *21st IAHR International Symposium on Ice "Ice Research for a Sustainable Environment, Dalian University of Technology Press, Dalian, China, June 11 to 15, 2012*. [Cited on page(s): 21]
- Maligno, A., S. Rajaratnam, S. Leen, and E. Williams (2010). A three-dimensional (3D) numerical study of fatigue crack growth using remeshing techniques. *Engineering Fracture Mechanics* 77(1), pp. 94–111. [Cited on page(s): 17]
- Malvar, L. J. and M. E. Fourney (1990). A three dimensional application of the smeared

- crack approach. *Engineering Fracture Mechanics* 35(1–3), pp. 251–260. [Cited on page(s): 18]
- Martins da Silva, L. and A. Öchsner (2008). *Modeling of adhesively bonded joints*. Springer. [Cited on page(s): 3]
- McClung, R. C. and J. C. Newman (1999). *Advances in Fatigue Crack Closure Measurement and Analysis: Second Volume*. ASTM International. [Cited on page(s): 1]
- Melenk, J. and I. Babuška (1996). The partition of unity finite element method: Basic theory and applications. *Applied Mechanics and Engineering* 39, 289–3146. [Cited on page(s): 22]
- Menk, A. and S. Bordas (2010). Crack growth calculations in solder joints based on microstructural phenomena with XFEM. *Computational Materials Science*. [Cited on page(s): 20]
- Moës, N. and T. Belytschko (2002). Extended finite element method for cohesive crack growth. *Engineering Fracture Mechanics* 69(7), 813–833. [Cited on page(s): 22]
- Moës, N., J. Dolbow, and T. Belytschko (1999, feb). A Finite Element Method for Crack Growth Without Remeshing. *International Journal for Numerical Methods in Engineering* 46, 131–150. [Cited on page(s): 19]
- Mohammadi, S. (2012). *Static Fracture Analysis of Composites*. John Wiley & Sons. [Cited on page(s): 19]
- Mubashar, A., I. A. Ashcroft, and A. D. Crocombe (2014). Modelling Damage and Failure in Adhesive Joints Using A Combined XFEM-Cohesive Element Methodology. *The Journal of Adhesion* 90(8), 682–697. [Cited on page(s): 1, 3]
- Odi, R. and C. Friend (2004). An improved 2D model for bonded composite joints. *International journal of adhesion and adhesives* 24(5), pp. 389–405. [Cited on page(s): 5]
- Park, K. and G. H. Paulino (2007). Cohesive Zone Models: A Critical Review of Traction-Separation Relationships Across Fracture Surfaces. *CASA report* 7(03). [Cited on page(s): 21]
- Pocius, A. (2002). *Adhesion Science and Engineering: Surfaces, Chemistry and Applications* (1 ed.). Elsevier. [Cited on page(s): 6]
- Pommier, S., A. Gravouil, N. Moës, and A. Combescure (2010). *Extended Finite Element Method for Crack Propagation* (1 ed.). Wiley-ISTE. [Cited on page(s): 1, 12, 15]
- Rabczuk, T. and T. Belytschko (2007). "A three-dimensional large deformation meshfree method for arbitrary evolving cracks. *Computer Methods in Applied Mechanics and Engineering* 196(29-30), pp. 2777–2799. [Cited on page(s): 17]

- Richardson, C., J. Hegemann, E. Sifakis, J. Hellrung, and J. Teran (2009). Simulating crack propagation with xfem and a hybrid mesh, I. *J. Numer. Methods Eng., submitted for publication*. [Cited on page(s): 19, 20]
- Robinson, P. and D. Q. Song (1992). A modified DCB specimen for mode I testing of multidirectional laminates. *Journal of Composite Materials* 26(11), pp. 1554–1577. [Cited on page(s): 10, 48, 52, 54]
- Simulia (2014). *ABAQUS 6.14 User Documentation*. [Cited on page(s): 47]
- Song, K., C. G. Davila, and C. A. Rose (2008). Guidelines and Parameter Selection for the Simulation of Progressive Delamination. [Cited on page(s): 10, 48, 62]
- Song, S. H., G. H. Paulino, and W. G. Buttlar (2006). A bilinear cohesive zone model tailored for fracture of asphalt concrete considering viscoelastic bulk material. *Engineering Fracture Mechanics* 73(18), 2829–2848. [Cited on page(s): 22]
- Systèmes, D. (2012). *Abaqus Documentation: Keywords Manual*. [Cited on page(s): 47]
- Vigneron, L. M., M. P. Duflot, P. A. Robe, S. K. Warfield, and J. G. Verly (2009). 2D XFEM-based modeling of retraction and successive resections for preoperative image update. *Computer Aided Surgery* 14, pp. 1–20. [Cited on page(s): 19]
- Xiao, Q. Z. and B. L. Karihaloo (2014). Implementation of hybrid crack element on a general finite element mesh and in combination with XFEM. *Computer Methods in Applied Mechanics and Engineering*, pp. 1864–1873. [Cited on page(s): 20]
- Xu, X.-P. and A. Needleman (1994). Numerical simulations of fast crack growth in brittle solids. *Journal of the Mechanics and Physics of Solids* 42(9), 1397–1434. [Cited on page(s): 22]
- Zavattieri, P. and H. Espinosa (2001). Grain level analysis of crack initiation and propagation in brittle materials. *Acta Materialia* 49(20), 4291–4311. [Cited on page(s): 22]

Vita

Emmanuel Irizarry Zapata

Emmanuel Irizarry was born in Mayagüez, Puerto Rico on February 19, 1986. After completing his education at Inés María Mendoza High School he was accepted at University of Puerto Rico Mayagüez campus mechanical engineering program.

In May 2011, he graduated obtaining a Bachelor Science degree in Mechanical Engineering. His interest in structural mechanics motivated him to join Dr. Goyal's research group in 2011 pursuing the masters degree in Mechanical Engineering at UPRM under the guidance of Dr. Vijay K Goyal.

During his M.S. degree experience, he worked as Teaching Instructor of several engineering courses related to Engineering Graphics and the Development of 3D models using Siemens NX Software. Also has been the recipient of the Departmental's Graduate Teaching Assistant for Mechanical Engineering undergraduate laboratories.

He expects to complete his M.S. degree one December 2015.